Tampere University

Marika Oksanen

THE ASSOCIATION OF CLAUDIN-19 WITH HUMAN EMBRYONIC STEM CELL -DERIVED RETINAL PIGMENT EPITHELIUM PRIMARY CILIA

Faculty of Medicine and Health Technology
Master's thesis
April 2020

Pro Gradu -tutkielma

Paikka: TAMPEREEN YLIOPISTO, Lääketieteen ja terveysteknologian tiedekunta
Tekijä: OKSANEN MARIKA SUVI HANNELE
Otsikko: Klaudiini-19 proteiinin yhteys ihmisen alkion kantasoluista erilaistettujen verkkokalvon pigmenttiepiteelisolujen primääri silioihin
Sivumäärä: 51
Ohjaajat: FM Taina Viheriälä ja FT Tanja Ilmarinen
Tarkastajat: FM Taina Viheriälä ja apulaisprofessori Vesa Hytönen
Päiväys: 24.4.2020

Tiivistelmä

Tutkimuksen tausta ja tavoitteet: Verkkokalvon pigmenttiepiteelin yleisin klaudiini proteiini on klaudiini-19. Aikaisemmin on tehty vain harvoja havaintoja klaudiinien sijainnista silioissa, eikä klaudiineille ole löydetty tehtävää siellä. Ryhmämme aikaisemmassa tutkimuksessa on havaittu klaudiini-19 proteiinin sijoittuvan solujen kehitykselle tärkeään sensoriseen värekarvaan, primääri siliaan (engl. primary cilium) kantasoluista erilaistettujen verkkokalvon pigmenttiepiteelin solujen maturaatiossa ja tiettyjen stimulusten, kuten epiteeli-mesenkyymi transition vaikutuksesta. Tämän tutkimuksen tarkoituksena oli selvittää klaudiini-19 proteiinin rooli ja tarkempi sitoutumispaikka primääri siliassa. Lisäksi tarkoituksena oli selvittää, vaikuttaako epiteeli-mesenkyymi transitio klaudiini-19 proteiinin sijoittumiseen primääri siliaan.

Tutkimusmenetelmät: Klaudiini-19 proteiinin roolia primääri silioissa tutkittiin hiljentämällä hetkellisesti sen luentaa. Proteiinin ilmentymisen muutosta seurattiin Western blot -menetelmällä. Lisäksi tutkittiin, onko TGF-β2 altistuksella vaikutusta proteiinin sijoittumiseen primääri siliaan. Altistuksen avulla tutkittiin myös klaudiini-19 proteiinin tarkempaa sijoittumiskohtaa primääri silioissa. Solut värjättiin klaudiini-19 ja primääri silia markkeriproteiinien vasta-aineilla, ja kuvannettiin käyttäen konfokaali- ja ekspansiomikroskopiaa.

Tutkimustulokset: Klaudiini-19 proteiinin vaikutusta primääri silioiden ylläpitoon ei saatu selville, sillä proteiinin hiljentämisessä ei onnistuttu. Proteiinin tarkkaa sijoittumista primääri silian rakenteessa ei saatu selville, mutta todettiin, että epiteeli-mesenkyymi transitio lisää klaudiini-19 proteiinin sijoittumista primääri siliaan.

Johtopäätelmät: Tutkimuksen aikana optimoitiin monia erilaisia tutkimusmenetelmiä, ja Western blot -analyysille, epiteeli-mesenkyymi transition induktiolle ja ekspansiomikroskopialle tehtiin protokollat. Tämä tutkimus osoitti, että klaudiini-19 proteiini ajoittain sijoittuu primääri siliaan. Kirjallisuudesta on havaittu yhtäläisyyksiä klaudiini-19 proteiiniin liittyvien sairauksien ja primääri siliaan liittyvien sairauksien välillä. Täten on mahdollista, että klaudiini-19 proteiinilla on rooli primääri siliassa, vaikka sitä ei tämän tutkimuksen aikana saatu selville.

Master's Thesis

Place: TAMPERE UNIVERSITY, Faculty of Medicine and Health Technology
Author: OKSANEN MARIKA SUVI HANNELE
Title: The association of claudin-19 with human embryonic stem cell-derived retinal pigment epithelium primary cilia
Pages: 51
Supervisors: MSc Taina Viheriälä and PhD Tanja Ilmarinen
Reviewers: MSc Taina Viheriälä and Associate Professor Vesa Hytönen
Date: 24.4.2020

Abstract

Background and aims: Claudin-19 is the most abundant claudin protein in human retinal pigment epithelia. There have been only few observations of ciliary localization of claudin-19, and its role in developmentally important primary cilia has not yet been established. Our previous work has identified that human embryonic stem cell derived retinal pigment epithelial cells possess claudin-19 immunopositive primary cilia during cell maturation and after certain stimuli, such as epithelial-mesenchymal transition. The aim of this study was to establish the role and more precise location of claudin-19 in primary cilia and also, whether epithelial-mesenchymal transition affects ciliary localization of claudin-19.

Methods: The role of claudin-19 in primary cilia was studied by transiently knocking down its expression with RNA interference. The change in protein levels was examined with Western blot. It was studied whether inducing cells to epithelial mesenchymal transition with TGF-β2 treatment would increase claudin-19 localization in primary cilia and also it was used to find the precise localization site within primary cilia. The cells were immunostained against claudin-19 and ciliary marker protein and imaged using confocal and expansion microscopy.

Results: It was not verified whether the claudin-19 knockdown would affect primary cilia maintenance, as the claudin-19 knockdown was not successful. The exact localization of claudin-19 in primary cilia was not identified, but it was shown that epithelial-mesenchymal transition induces claudin-19 localization in primary cilia.

Conclusion: There were several different methods optimized during the study and protocols for Western blot, epithelial-mesenchymal transition induction, and expansion microscopy were established. This study showed that claudin-19 is occasionally located in primary cilia. It has been noticed from previous studies that claudin-19 associated diseases and primary cilia associated diseases have some similarities. Based on this evidence it is possible that claudin-19 has a meaning and role in primary cilia, even though it was not verified in this study.

Acknowledgements

This thesis work was carried out in the Eye group, Faculty of Medicine and Health Technology, Tampere University, Finland. I would like to address my deepest gratitude to the group leader Heli Skottman for giving me the opportunity to be a part of her group and perform my thesis project in this fascinating field of science.

I wish to acknowledge my supervisors Tanja Ilmarinen and Taina Viheriälä. Thank you for your help on every step on the way of this project. For Tanja I would like to mention her strong expertise in making science and always having time for me even during her busy days. For Taina I am grateful that she was willing to supervise me even during her maternity leave and for taking me under her wing from the day one when I came to this group.

I also want to thank our group members Outi Melin and Hanna Pekkanen for sharing their expertise in technical issues and Maija Kauppila and Meri Vattulainen for helping me every time I had “just a quick question”. I am grateful to Heidi Hongisto for teaching me Western blotting and for always cheering me up when I was losing hope with this project. I wish to thank Toni Montonen who walked me through expansion microscopy with a smile on his face. Lastly, I want to thank the whole Eye group for the amazing atmosphere and friendship. It means everything to me.

Tampere, April 2020

Marika Oksanen

Table of contents

Abbreviations

α-SMA	Alpha-smooth muscle actin
3D	Three dimensional
Acrolyl X-SE	6-((acrolyl)amino)hexanoic acid succinimidyl ester
AMD	Age-related macular degeneration
APS	Ammonium persulfate
ARL13B	ADP-ribosylation factor-like protein 13B
ARPE-19	Adult retinal pigment epithelial cell line-19
BBC	Basal body complex
BSA	Bovine serum albumin
CIV	Collagen-4
CL2	Claudin-2 protein
CL19	Claudin-19 protein
CLDN19	Claudin-19 gene
DAPI	4′,6-diamidino-2-phenylindole
DPBS	Dulbecco's phosphate-buffered saline
DTT	Dithiothreitol
EDTA	Ethylenediaminetetraacetic acid
EMT	Epithelial-mesenchymal transition
ExM	Expansion microscopy
hESC-RPE	Human embryonic stem cell -derived retinal pigment epithelium
hf-RPE	Human fetal retinal pigment epithelium
Hh	Hedgehog signaling pathway
hPSC	Human pluripotent stem cell
IF	Immunofluorescence
iPSC	Induced pluripotent stem cell
KO-DMEM	KnockOut™ Dulbecco's modified eagle's medium
LN521	Laminin-521
LSCM	Laser scanning confocal microscopy
MDCK	Madin-Darby canine kidney
MIP	Maximum intensity projection

MTOC	Microtubule-organizing center
PFA	Paraformaldehyde
PTM	Post translational modification
PVDF	Polyvinylidene difluoride
RIPA	Radioimmunoprecipitation assay
RNAi	RNA interference
RPE	Retinal pigment epithelium
RT	Room temperature
SDS-PAGE	Sodium dodecyl sulfate-polyacrylamide gel electrophoresis
siRNA	Short interfering RNA
TBS	Tris buffered saline
TBS-Tween	Tween20 in tris buffered saline
TEER	Transepithelial electrical resistance
TEMED	Tetramethylethylenediamine
TGF-β2	Transforming growth factor-beta 2
WB	Western blot
XF-KO-SR	KnockOut™ SR XenoFree CTS™
ZO-1	Zonula occludens-1

1 Introduction

Retinal pigment epithelium (RPE) is a monolayer of cells located between neural retina and the choroid in the retina of the eye. It has several important roles in visual function, including light absorption, epithelial transport and maintaining the visual cycle.[1] RPE is a tight epithelium that has several cell-cell junctions, including tight junctions. One major tight junction protein family is claudin proteins from which claudin-19 (CL19) has a role in determining the permeability and selectivity in human RPE tight junctions.[2]

Cilia are microtubule-based protrusions in the apical side of almost every vertebrate cell type. Primary cilia are non-motile, and their structure consists of nine outer microtubule doublets, but they lack the central pair that motile cilia have. Primary cilia are functioning as signaling hubs and they are crucial in development of several organs. After developmental phases, they usually diminish. Nevertheless, some cell types remain ciliated during adulthood as well.[3]

There are a few observations of localization of claudin proteins in primary cilia.[4,5] The role of CL19 in primary cilia is not established, but claudin-7b and claudin-h downregulation has been observed to lead to abnormalities in primary cilia structure in the kidney.[5] However, CL19 mutation leads to Familial primary hypomagnesemia with hypercalciuria and nephrocalcinosis with severe ocular involvement. It is a serious disease that has onset already in childhood, which indicates problems in developmental biology.[6] On the other hand, primary cilia are needed in normal development. Therefore, it can be said that *CLDN19* mutations lead to conditions that resemble diseases caused by deficiencies in primary cilia (ciliopathies). It is possible that the RPE cells of patients with *CLDN19* mutations are not maturing normally, because primary cilia are needed in their normal maturation.[7] These aspects suggest that there could be a link between CL19 and ciliopathies. In our previous data, we have observed how CL19 localizes to primary cilia during maturation of human embryonic stem cell –derived RPE (hESC-RPE) and after certain stimuli. This evidence leads to the hypothesis that CL19 could be involved with primary cilia.

Studying primary cilia has expanded over the years because of their roles in vertebrate development and association in human genetic diseases.[8] Because of the recent interest in studying primary cilia, several new cilia associated proteins have been found. Nevertheless, numerous cilia-associated proteins with unknown function in primary cilia remain.[9] This thesis is trying to answer the question, whether CL19 has a role in hESC-RPE primary cilia.

2 Literature review

2.1 Retinal pigment epithelium

RPE is a monolayer of cuboidal cells beneath neural retina structure, located in the back of the eye between photoreceptor outer segments and the blood vessels of the choroid (Figure 1). The fact that the RPE is facing a solid tissue on its apical side and forms a blood-tissue barrier makes it special among other epithelia.[2] It mainly functions in maintaining the visual cycle by for example light absorption, recycling photoreceptor outer segments and controlling transport of nutrients and metabolic waste from the retina to bloodstream and the other way around.[1] Different forms of retinal degeneration diseases can begin with degeneration or malfunction of the RPE. Therefore, RPE has become widely studied as researchers are trying to establish stem cell-based treatments to retinal degeneration.

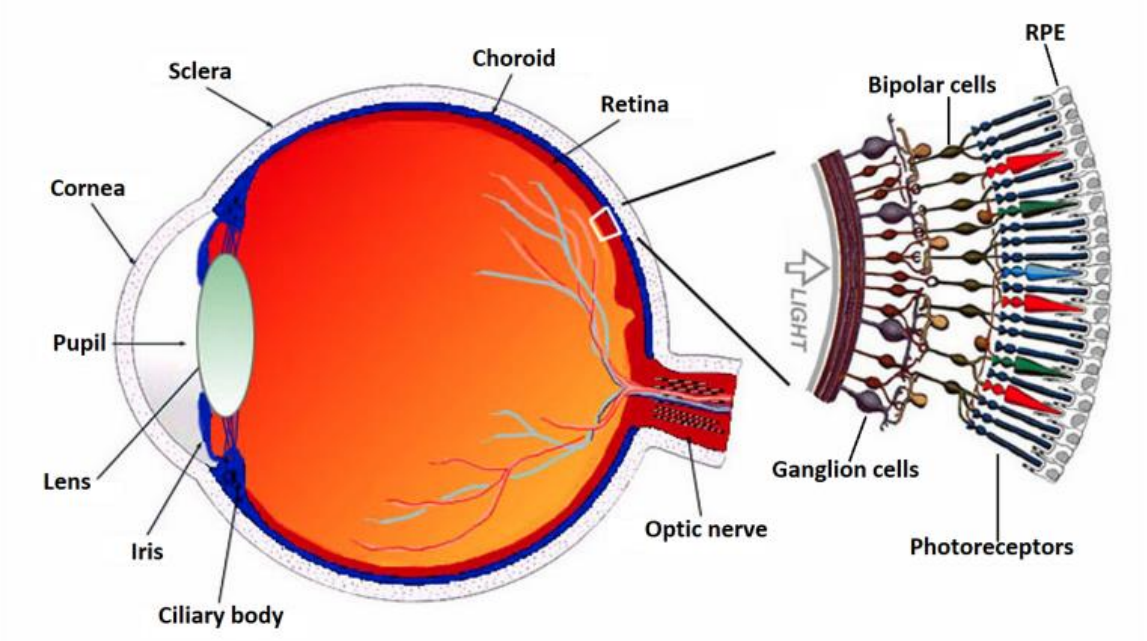

Figure 1. The structure of the human eye with schematic enlargement. RPE cells' long microvilli are facing photoreceptor outer segments. RPE is laying on top of the choroid, that is not illustrated. By forming a solid barrier between blood vessels of the choroid and other tissues of the eye, RPE has an important role as a blood-tissue barrier. (Modified from https://webvision.med.utah.edu/book/part-i-foundations/simple-anatomy-of-the-retina:18.2.2020).

RPE cells are organized in a mosaic-like structure from hexagon-shaped cells, that is thought to be the most energetically favorable cell-arrangement. The RPE cells' apical membrane has long microvilli that are surrounding photoreceptor outer segments. Basal membrane of RPE is facing the Bruch's membrane, that physically separates retina from choroid. The basal plasma

membrane of RPE cells contains several infoldings that increase the surface area of membrane and enhances transport.[10] RPE cells have pigment melanin granules that cause their characteristic dark color.[1,10] These granules are called melanosomes and they are lysosome-like compartments that are specialized to synthetize and store melanin.[11] RPE contains several cell junctions, including desmosomes and hemidesmosome-like structures between basal plasma membrane and Bruch's membrane and tight-, adherens- and gap junctions and occasional desmosomes between adjacent RPE cells. These junctions permit paracellular permeability, cellular integrity and cell-cell contact.[10] Without several cell junctions, RPE could not serve its functions that demand an intact epithelium.[12]

2.1.1 Functions of Retinal pigment epithelium

RPE has several functions in maintaining health and integrity of the distal retina and choroid[13] (Figure 2). RPE's primary functions are in forming the outer blood-retina barrier and maintaining the visual cycle by ensuring correct composition of the sub-retinal space and separating capillaries of the choroid from the neural retina. Different forms of retinal degeneration and eventually loss of vision are possible outcomes, if the functions of RPE are disrupted.[1]

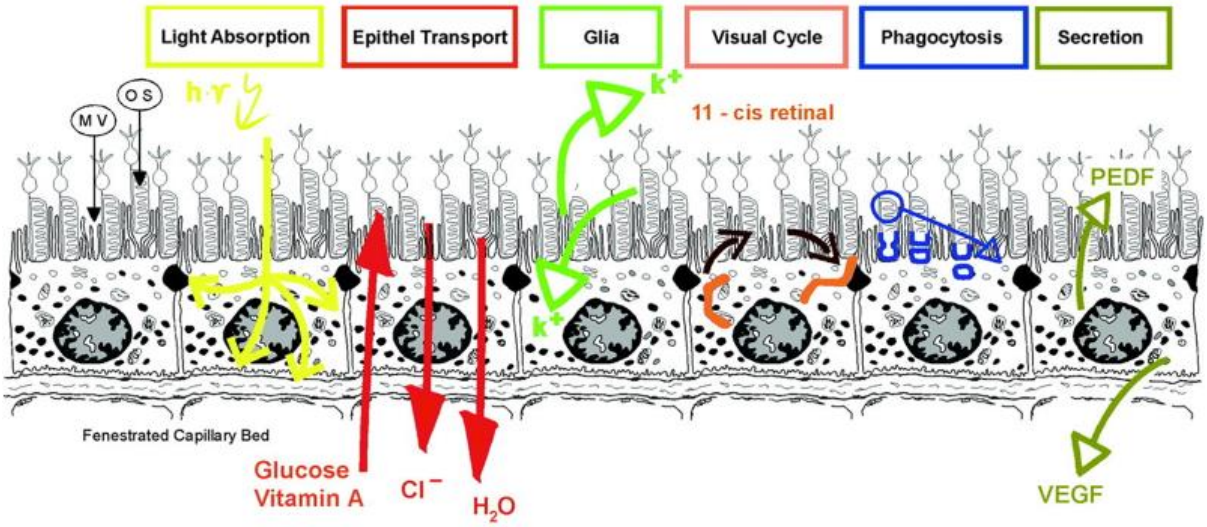

Figure 2. The most important functions of RPE. RPE absorbs light energy, transports molecules and ions, performs spatial ion buffering, maintains visual cycle by transforming retinol to retinal, phagocytoses photoreceptor outer segments and secretes growth factors to control nearby tissues. Modified from reference 1.

RPE cells absorb the light energy that is refracted to the retina. The amount of energy could cause damage to the eye if it was not absorbed. Therefore, the light absorption to pigmented

melanin granules is protecting the cells from photo-oxidative stress and damage.[1,14] RPE cells enable transepithelial transport of water, ions and nutrients from blood to photoreceptor cells and from subretinal space to blood. For visual function it is crucial to transport water out of the subretinal space.[1,11] Water accumulates into the retina due to metabolic reactions and intraocular pressure that loads water from vitreous body to the retina.[1] RPE pumps the water out together with Cl^- and K^+ ions. This transport is provided with the energy from Na^+-K^+-ATPases located in the apical membrane of RPE cells. RPE also have exchangers for lactic acid and bicarbonate. Therefore, RPE also controls the pH of subretinal space with this transport machinery. In addition to ions and water, RPE transports metabolic end products from subretinal space to blood and nutrients such as glucose, retinol and fatty acids from blood to photoreceptors.[1,11] Retinol is not only transported, but it is constantly exchanged between RPE and photoreceptors. This is because photoreceptors cannot reisomerize retinol to retinal. After photoisomerization of 11-cis-retinal to all-trans-retinal, the latter is reduced to all-trans-retinol and transported from photoreceptors to RPE. RPE transforms it to 11-cis-retinal that is transported to photoreceptors in a usable conformation.[15] Furthermore, RPE maintains photoreceptor function by stabilizing the ion composition in the subretinal space and by phagocytosing, digesting and recycling the shed photoreceptor outer segment components. Finally, RPE secretes several growth factors that maintain stability and structure of choriocapillaris endothelium, photoreceptors and retinal neurons.[16] RPE also secretes immunosuppressive factors that have a role in establishing the immune privilege of the eye.[1,17] If these functions are somehow altered or loss, it can lead to several forms of retinal degeneration.

2.1.2 Retinal degeneration; treatment and disease modeling

As indicated, RPE has several vital functions in maintaining the visual cycle and viability of surrounding tissues. Disrupting the RPE disturbs normal fluid flow between choriocapillaris and neural retina, which results in buildup of fluid, called edemas. However, this also alters the metabolic circuits and function of the RPE itself.[12] Therefore, it is understandable that the loss of functional RPE cells leads eventually to loss of vision.

There are tens of millions of individuals affected by retinal degenerative diseases worldwide.[18] These diseases are rising from several different disease mechanisms and genes that are not functioning properly. Therefore, there are also several different approaches to treat retinal diseases, for example gene therapies, photodynamic therapy, angiostatic steroids, growth factor suppressors and the artificial retina.[19] Nonetheless, there are diseases that are untreatable with

these approaches, for example a dry form of age-related macular degeneration (AMD). In the AMD, the macula of the eye degenerates, which leads to a loss of central vision.[18] Wet form of the AMD can be treated but not cured with intraocular antibody injections, but there are no effective options to treat the dry AMD.[14,18] Therefore, there is a need for new therapy approaches, from which the cell replacement therapy is a tempting option. It is particularly tempting for the RPE degeneration, as the RPE structure is relatively simple; a monolayer of cells laying on Bruch's membrane.[18] This approach could not only treat the symptoms but also restore visual function, if the photoreceptors remained viable before starting the treatment. Nevertheless, there have been indicated several obstacles in RPE cell replacement therapies; i) will the transplanted RPE cells survive on diseased Bruch's membrane, ii) how the cells are delivered to subretinal space, iii) how to ensure transplant integration to target site, iv) how to prevent immune rejection of the allogenic transplant, and v) how to prevent cells from vigorously proliferating and emerging tumors and cancer.[20] All these pitfalls must be solved, before cell replacement therapies can be used in treatment of retinal degeneration.

Cell replacement therapies are currently targeted to treat common retinal degeneration diseases. However, each disease has its own characteristics and they require specific treatment options. Therefore, disease models have to be developed to further study specific diseases.[21] Animal models were previously used, but their usage is restricted by ethical issues and the critical differences between humans and other animals. For example, some common rodent animal models are not that usable in eye research, as they lack the macular region found in human.[21] Cell culture -based disease models are preferred over animal models as the results are more easier to reproduce and the experimental system can be easily controlled and manipulated.[22] Stem cell technology enables *in vitro* disease modeling with for example human pluripotent stem cells (hPSC) that are widely used and efficient in studying several different cell types of the human body. RPE generated from hPSCs is a novel tool to study and understand RPE cells function and eventually RPE related retinal degeneration diseases.[23] Nevertheless, the usage of human embryos brings ethical issues to research. A technique to reprogram fully differentiated somatic cells to induced pluripotent stem cells (iPSC) was established in 2006.[24] iPSCs are similar to hPSC in their morphology, proliferation, differentiation capacity and genomic and epigenomic states.[25] Therefore, iPSCs have wide possibilities in basic research, drug screening, disease modeling, toxicological studies and cell therapy.[26] The ethical issues from using human embryos are eliminated, as iPSCs can be produced from easily accessible cell types for example, blood cells, keratinocytes and dermal fibroblasts.[27] Furthermore, iPSCs make it possible to

study inherited diseases in detail from the patient cells *in vitro*. By differentiating RPE cells from iPSC, several different RPE related retinal degenerations can be studied.[21]

2.2 Claudin proteins

Different compositions are separated by epithelial sheets in organisms that have higher structures.[28] It is strictly regulated which molecules can be transported through these epithelia and in what pace. In vertebrates, this regulation is mainly controlled by tight junctions.[28,29] A tight junction is a form of cell junctions, that is responsible for maintaining the paracellular barrier for large molecules and controlling the paracellular transport of ions.[30] They are formed by a complex of transmembrane and peripheral proteins that are connected to the cell cytoskeleton.[28] Each epithelium requires different barrier properties to suit its function in a certain location of a human body. These different properties are arising from different contributions of tight junction proteins.

The structure of different claudins is relatively conserved. They have four hydrophobic transmembrane domains that anchor them to the cell membrane.[31] The intracellular domain is short, only 7 amino acids, whereas the cytoplasmic domain is longer 40-70 amino acids. The length of the cytoplasmic tail is the biggest difference among claudin proteins, and presumably it is the aspect that at least partly explains each claudin's different paracellular selectivity properties. These cytoplasmic tails include a PDZ-binding domain, that directly binds certain proteins. Zonula occludens-1 (ZO-1) is a well-known cytoplasmic scaffold protein in human RPE. Claudins are anchored to cell membrane when they bind ZO-1. By this manner, claudins get linked to actin cytoskeleton and simultaneously stabilize the formed tight junctions on cell membranes.[31,32]

Claudin proteins are the most abundant tight junction proteins in human epithelia. They are mainly responsible for maintaining epithelia's ion selectivity.[31] There is a total of 27 different claudin proteins encoded by the mammalian genome[33] and each of them is bringing different contribution to the ion selectivity.[30] Therefore, each epithelium has characteristic subset of claudins. In addition to the subset of claudin proteins, the way they are co-polymerized affects the properties of the given epithelium.[34]

The role of claudins in establishing semi-selectivity of epithelia occurs by forming aqueous pores to tight junction structure. Inside the pore, the claudins interact with charged ions either to prevent or permit their passing through the epithelium. This ability to select which ions can pass, comes from the claudin amino acid sequence and their charges that are lining the pore.

Claudin protein family is divided into groups based on their ability to either form a barrier or to form a pore structure. They can be classified to claudins that predominantly restrict or permit anion/cation permeability through the junction.[35]

2.2.1 Claudin-19

CL19 is a member of the claudin protein family and it is expressed by peripheral nervous system, kidney and RPE.[35,36] It is the most abundant claudin protein in human RPE,[2] which makes it interesting for human eye research. It determines the permeability and semi-selectivity of tight junctions in the tissues it is expressed. It mainly functions as a barrier against anions.[35] Nevertheless, there is also some data that indicate its role as a sodium ion barrier.[37] Furthermore, it has recently been detected to regulate the expression of barrier related pathway proteins in RPE cells.[38] CL19 also regulates genes that are encoding retinal neurotrophic factors and proteins of the visual cycle.[36] It is notable, that decreased expression levels of a RPE maturation marker Retinal pigment epithelium-specific 65 kDa protein have been observed with both defective primary cilia[7] and *CLDN19* mutations.[36]

Mutations of *CLDN19* has pleiotropic effects, meaning that a single mutation has multiple effects in the human eye. For example, they cause macular colobomata, myopia and horizontal nystagmus.[6] In addition, one of the best-known conditions of *CLDN19* mutations is Familial primary hypomagnesemia with hypercalcuria and neprocalcinosis. In general, renal magnesium and calcium wasting in the kidney occurs in this condition. In the kidney, and more precisely in the thick ascending limb of Henle's loop, claudin-16 and CL19 are forming heteromultimers and are responsible for magnesium and calcium ion reabsorption. A mutation in either of these genes leads to the condition, but only *CLDN19* mutations lead to ocular involvement. This is understandable as claudin-16 is not expressed in the RPE.[6,38]

2.3 Primary cilia

Cilia are microtubule-based cell compartments that are protruding from the apical surface of several cell types. In addition to RPE cells, primary cilia are found on other epithelial cells, for example kidney tubule, endocrine pancreas and thyroid. Other cell types than epithelial cells can produce primary cilia as well. These include for example Schwann cells, fibroblasts and neurons.[39] There exist two types of cilia, motile and non-motile, from which the non-motile cilia are called primary cilia.[3,40] In recent years, the role of primary cilia has been better understood. They primarily function as signaling hubs in developmental phases after which they diminish, but some cell types remain ciliated during adulthood as well. However, primary

cilia have not been observed in mature RPE cells.[3] Well-known signaling pathway proteins that localize in primary cilia are Hedgehog (Hh) and Wingless. Their primary roles are in regulating embryonic development and this further emphasizes primary cilium's developmental roles.[39]

2.3.1 Structure

The structure of cilia is composed of microtubule skeleton called axoneme, that is surrounded by a ciliary membrane (Figure 3). Primary cilia have a specific microtubule-organizing center (MTOC) that is called a basal body. In addition, there are smaller compartments in the structure of primary cilia, including transition zone, Y-linkers and ciliary tip.

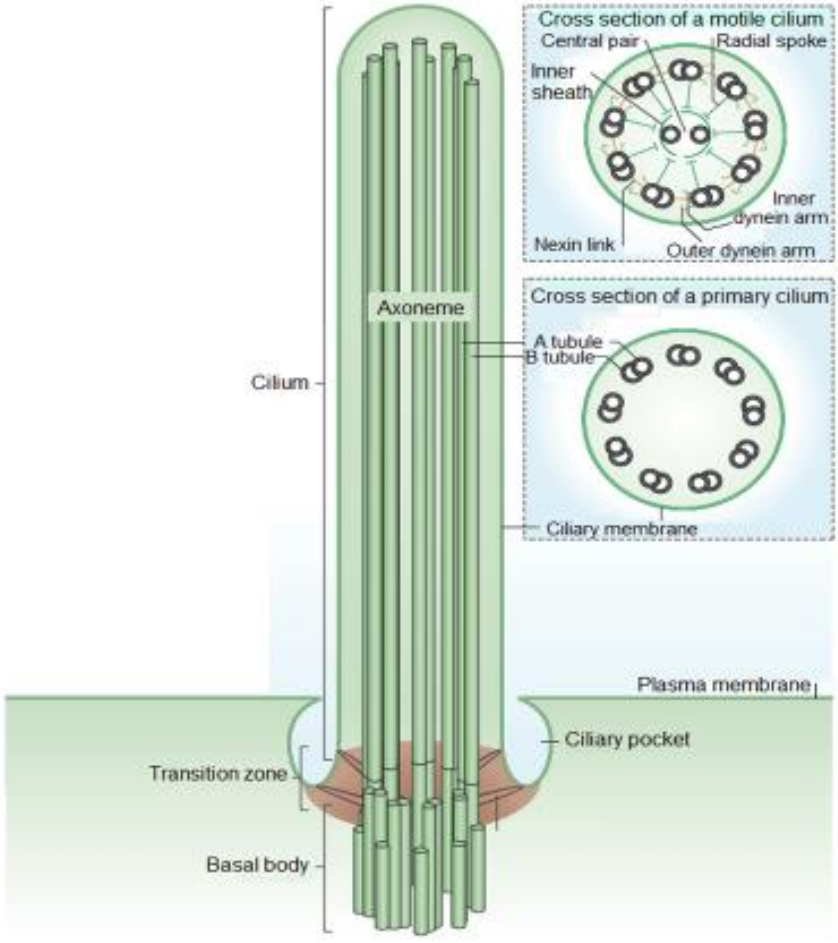

Figure 3. Structure and cross sections of motile and non-motile cilia. Microtubule pairs that form the axoneme are made up by one whole microtubule (A tubule) that is connected to an incomplete microtubule (B tubule).[3,9] Basal body is anchored to immediate proximity to plasma membrane, where it functions as MTOC elongating the axoneme and stabilizing primary cilium's location into one place. Transition zone separates ciliary membrane from plasma membrane and ensures specific lipid composition that is crucial for primary cilium's functionality.[7,41] Modified from reference 9.

The aspect that enables different motility properties between motile and non-motile primary cilia is their microtubule structure. Motile cilia have 9+2 microtubule axoneme, consisting of nine microtubule doublets that form a cylinder structure, and inside the cylinder, there are two microtubules. Non-motile cilia lack this inner doublet. Therefore, their axoneme is referred as 9+0.[3,40] There are also some exceptions in motility properties of 9+2 and 9+0 cilia, but the basic rule is as described.[3,8] In addition to tubulin, there are also other components in the axoneme. These are tektins and protofilament ribbon proteins and their supposed role is to bring stability to the cilia. These structural components might explain why axoneme microtubules do not disassemble spontaneously *in vitro*. Ciliary membrane surrounding the axoneme is continuous with plasma membrane but still a distinct unit from it. The ciliary membrane contains several different receptor proteins that link primary cilia to different cell signaling routes.[40-42]

Basal body is a modified form of the older centriole, called a mother. Division of the mother centriole during the previous S phase develops the daughter centriole.[9] The mother centriole and daughter centriole have both structural and biochemical differences between each other and mother centriole's characteristics enable it to nucleate the primary cilium.[43] Basal body's structure consists microtubule triplets, and axoneme is extending from two of the three microtubules. Mother and daughter centrioles together constitute the basal body complex (BBC).[3]

The transition zone is an important component of primary cilium as it is located on the critical site for ciliary function regulation at the bottom of the cilium. It connects axoneme to BBC and forms a diffusion barrier, which enables specific microenvironment inside primary cilium. The transition zone is surrounded by a specific periciliary membrane. The transition fibers in transition zone that connect microtubule doublets of the axoneme to the cell membrane is defined as Y-linkers.[3,43] The ciliary tip is an important detail in ciliary structure that maintain primary cilium's function. It is a specialized region with certain protein composition and ultrastructure. Different signaling pathway components accumulate there and the ciliary length is remodeled by adding or removing subunits at the tip.[3]

2.3.2 Ciliogenesis

Assembly of a new cilium, or ciliogenesis, requires several different steps that must be strictly regulated. There are three time points when cells can regulate primary cilia absence or presence; synthesis of precursors, transport and assembly of precursors and cilium turnover.[9] As the basal body is derived from the mother centriole, primary cilia form only in quiescent

cells or during G1 phase of the cell cycle[41,42] (Figure 4). This link to the cell cycle brings another level of regulation to ciliogenesis, as the cell cycle is one of the most strictly regulated processes in cells.[43] Other aspects that regulate ciliogenesis are cell confluence, fluid flow and cell spreading.[9]

The mother centriole requires some modification steps before it can be used as a basal body. There must form structures that are anchored to cytoplasmic microtubules called basal feet. These basal feet are derived from subdistal appendages of the mother centriole.[9,43] Without this anchoring of basal bodies, they are not sufficiently polarized inside cells.[9] Components of primary cilium, such as tubulin, must be synthetized inside the cytosol because protein synthesis does not occur inside the cilium.[42,43] This is one of the key regulation steps. It can be indicated by the fact that during primary cilia construction there are several hundreds of genes upregulated.[9] The synthetized primary cilium components must be transported to elongating primary cilium.[40,42,43] This process serves as an important control point of ciliogenesis, as the cargo size, speed, entry and selection are easily regulated parameters.[9]

The axoneme is not a static structure but rather dynamic. The length of cilia is not increasing, when the turnover rate is balanced with incorporation of new tubulin at the cilia tip.[9] One key protein in the regulation of ciliary length is ADP-ribosylation factor-like protein 13B (ARL13B). In the absence of this ciliary protein, the observed cilia lengths are significantly shorter compared to wild type. Correspondingly, cells that overexpress ARL13B has been shown to produce relatively long cilia.[44]

Primary cilium turnover must happen shortly before the cell enters mitosis.[39] Basal body must be transformed back to centrioles that are transported to cell interior. This ensures mitotic spindle formation and correct cell division.[43] There are two possible routes to primary cilium turnover specified in literature; whether the primary cilium is cleaved off from the basal body before further disassembly or it is actively disassembled by cooperation of different proteins.[9]

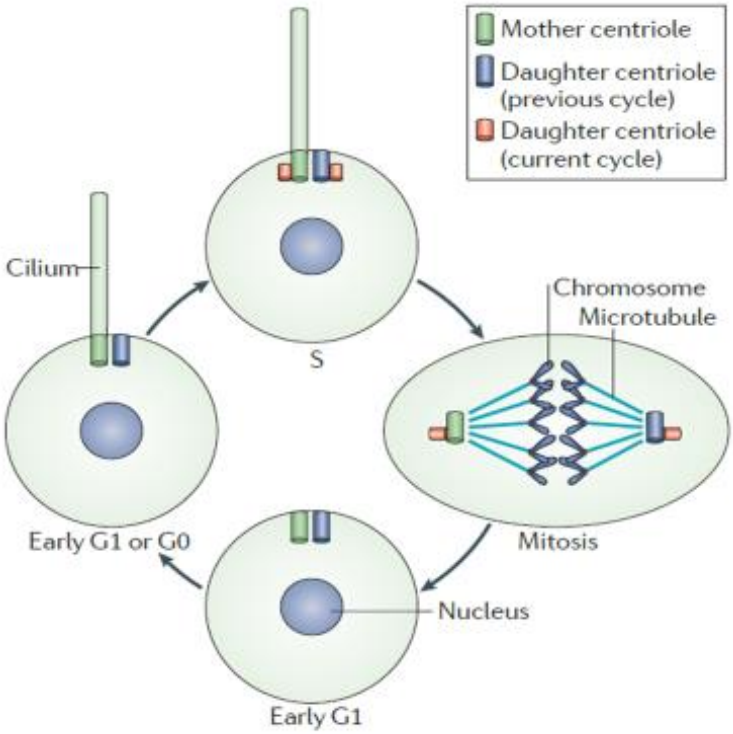

Figure 4. Primary cilium formation during cell cycle. Cells that are newly divided in early G1 phase do not possess primary cilia. Mother centriole docking to actin-rich cell cortex occurs during G1 and the primary cilium is nucleated. During S-phase the centrioles are duplicated and just before mitosis the primary cilium is resorbed. Therefore, the centriole pairs are allowed to detach from the cell cortex and perform their function in cell division. Primary cilium is re-formed again in G1. Modified from reference 9.

There are two possible pathways for assembly of a new primary cilia, extracellular and intracellular pathway (Figure 5). The extracellular pathway, that appears to be common among epithelial cells, is working through basal body's docking straight to the apical membrane[40,45], and more precisely onto the actin-rich cell cortex.[9] Therefore, primary cilium is constructed straight to extracellular space. On the contrary, intracellular pathway is well known for fibroblasts and smooth muscle cells, and it leads to ciliary pocket structures.[45] In this pathway, the basal body is docked to a vesicle, wherein primary cilium is produced. The vesicle together with a mature primary cilium is translocated to proximity of the apical membrane. Fusion of the vesicle and cell membrane leads to protrusion of the primary cilium towards extracellular space.[40,41,45] Usually in this pathway, the primary cilium remains partly invaginated by the membrane and is not fully exposed to the extracellular space. These invaginations are called ciliary pockets. For example, Madin-Darby canine kidney (MDCK) cells have been proved to possess only few ciliary pocket structures, whereas most RPE cells have primary cilia

protruding from ciliary pockets.[45] This aspect shows that RPE is an exceptional epithelium among others based on primary cilia formation.

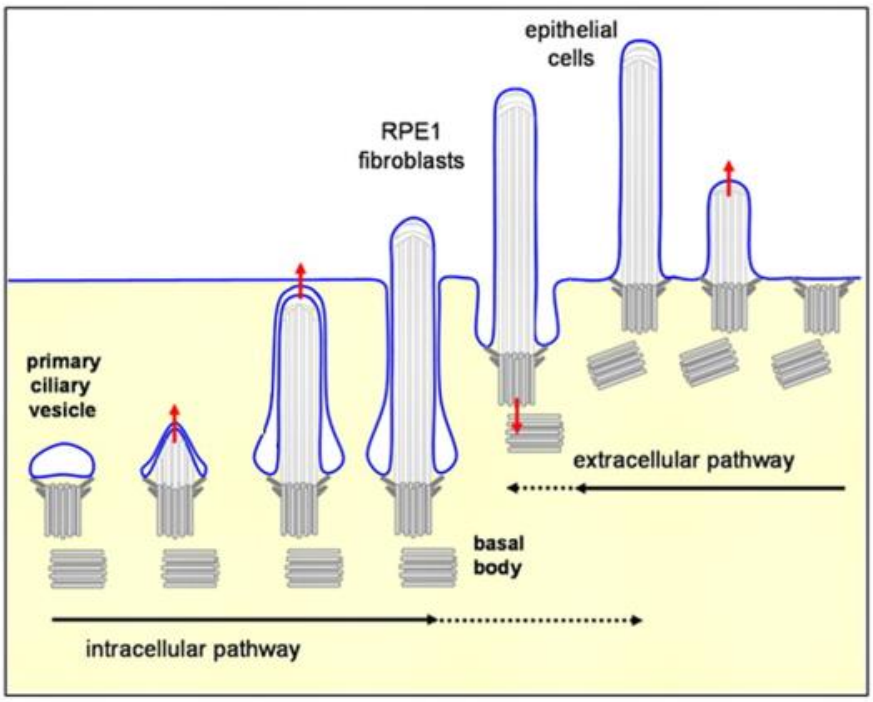

Figure 5. Ciliogenesis pathways. Intracellular pathway (left) is common for fibroblasts, smooth muscle cells and neurons but also RPE. In this pathway, primary cilium is elongated into primary ciliary vesicle. Eventually, this vesicle is fused with cell membrane and primary cilium gets protruded to extracellular space. In extracellular pathway, the basal body is docked straight to cell membrane, and forming primary cilium is constantly exposed to extracellular space. Modified from reference 45.

2.3.3 Function

There is a special microenvironment inside a primary cilium and on ciliary membrane. This microenvironment enables specific molecular interactions between signaling molecules, for example receptors, ligands and downstream transducers. This unique microenvironment enables primary cilia to function as a signaling hub.[9,46] Studies indicate that ciliary composition is kept unique by similar mechanisms that are used in neuronal axons. These include selective targeting, exclusion, retention, and diffusion barriers. Some proteins are transported in or out the cilium or kept inside the cilium by a specific manner. The base of the cilia maintains this unique microenvironment, since it is the only part of the cilium that is not covered by a membrane.[41] Basal body acts as a gatekeeper that regulates which downstream signaling events are able to happen after activation of ciliary receptors.[42] The association between the axonemal microtubules and membrane within transition zone forms a barrier that allows the selective

passage of materials into the cilium.[43] Therefore, both basal body and transition zone function in enabling sensory properties of primary cilia.

Primary cilia associated pathways control processes of embryogenesis, tumorigenesis, feeding behavior, kidney function, vision and smell.[41] The well-known signaling pathways that localize into primary cilia are for example Hh, Wingless, Fibroblast Growth Factor, Notch, mTOR and Platelet-derived Growth Factor signaling pathways.[42] Hh serves as an example on how signaling pathways function utilizing the microenvironment in primary cilia.

While inactive, Hh receptors are accumulated in ciliary membrane keeping the next downstream receptor inactive and located in cell membrane. When the first receptor binds Hh ligand, it gets inactivated and transported out of primary cilium. The next receptor protein can be transported to ciliary membrane, where it enables transcription factor activation. Transcription factor together with its inhibitor are located in primary cilium tip. When the inhibitor is inactivated, it dissociates from transcription factor. The active transcription factor can be translocated to nucleus where it activates its target gene's expression. This is a general example on how players of a signaling pathway can be recruited in primary cilium and how primary cilium is functioning as a signaling hub. As a conclusion, several signaling pathway components are separated from each other by localizing them to different compartments in or around primary cilium. After activation processes they are brought together resulting in gene expression regulation.[47,48]

In addition to serving as a signaling hub, primary cilium also functions as a cellular global positioning system and it detects changes in its environment. In this manner it can for example initiate cellular replacement after damage.[39] It is also indicated that ciliary length might affect primary ciliary functions as several cilium related diseases involve observations of alterations in ciliary length. For example, the ciliary length differs from normal in Retinitis pigmentosa.[9] In addition, the primary cilium length has been observed to be related in primary cilia's mechanosensitivity features. Mechanosensitivity is important in primary ciliary function, as it enables primary cilia to transmit external stimuli, for example fluid flow, to cells via cell signaling pathways.[49]

Physiological problems in primary cilia cause deregulation of signaling pathways that in downstream causes broad complications in organism level.[47,50] These problems often lead to severe developmental disorders, called ciliopathies. For example, defects in primary cilia cause cysts in kidney, liver and pancreas.[8] In other tissues it can cause anosmia, retinal degeneration,

obesity or polydactyly.[9] Problems in cell cycle regulation are also connected to primary cilia as ciliogenesis is strictly regulated together with the cell cycle. Therefore, it is understandable that defects in primary cilia are found in several cancers.[43] Studying and gaining extensive knowledge of primary cilia and their function may help in development of new treatments for ciliopathies.[50-52] For that reason, primary cilia have become notable research subject in cell biology in the last decade.[47]

2.3.4 Claudin in primary cilia

There are limited observations of claudin localization in primary cilia in general[4,5] and only one study showing this happening in RPE cells.[4] In this study, the used antibody was against claudin-1 and it was stated possible that it cross-reacts with claudin-3. Claudin immunopositive primary cilia were not detected in any other cells that were tested, including photoreceptor cells, epithelial cells of nasal mucosa, small intestine and colon. Therefore, the authors suggested that claudin positive primary cilia is a unique phenomenon in only RPE cells. Nevertheless, claudin-2 but not claudin-4 have been found in primary cilia of MCDK cells.[53] The localization of claudin in primary cilia has not been studied further to date. In our previous studies it has been shown that CL19 localizes to primary ciliua during hESC-RPE cell maturation. We have also observed that in certain circumstances the primary cilia are elongated with frequent observations of CL19, indicating that claudin serves some functions in primary cilia. These circumstances include certain stress inductions and in addition, fibrotic cells that are similar to cells in EMT possess these elongated and CL19 immunopositive primary cilia. Clearly, this is an issue that requires further studies.

3 Aims of the research

The first aim of the thesis work was to establish if CL19 is involved in elongating primary cilia. The hypothesis was that if CL19 has a role in primary cilia elongation, knocking down *CLDN19* either prevents the elongation or disrupts it so that the eventual length of the primary cilia is reduced. Decrease in expression of CL19 was verified by Western blot (WB). The second aim of the thesis was to investigate where CL19 is located in primary cilia. This was done by inducing cells to epithelial-mesenchymal transition (EMT) and microscopy methods using primary cilia specific marker proteins. These methods were also used in the third aim, that was to study whether EMT would increase CL19 localization in primary cilia. Microscopy methods that were used in this study were laser scanning confocal microscopy (LSCM) and expansion microscopy (ExM).

4 Materials and methods

4.1 Cell culture

The hESC cell lines used in this study were Regea08/017 and Regea08/023. They were derived, characterized and differentiated to RPE as previously described.[54,55] Tampere University has the approval of the National Supervisory Authority for Welfare and Health (Dnro 1426/32/300/05) to conduct research on human embryos. The institute also has supportive statements of the Ethical Committee of the Pirkanmaa Hospital District to derive, culture, and differentiate hESC lines (Skottman/R05116). No new hESC lines were derived for this study. The primary RPE cells used in this study were previously isolated and cryopreserved from porcine eyes acquired from the local abattoir as a side product of food production. The isolation was performed by previously described protocol.[56]

Previously differentiated and cryopreserved cells were thawed and plated to either porous, hanging cell culture inserts (polyethylene terephthalate coated, pore size 1.0µm, Sarstedt AG & Co. KG) with a density of 2.5×10^5 cells/cm^2, 6-well cell culture plates (Corning CellBIND; Corning Inc., USA) with a density of 1.1×10^5 cells/cm^2 or Thermanox Plastic Coverslips (Thermo Fisher Scientific Inc., USA) with a density of 1.0×10^5 cells/cm^2. Platforms were coated with laminin (1,8 ug/cm^2, LN521, Biolamina AB, Sweden) and collagen (CIV, 10 ug/cm^2, Sigma-Aldrich Co. Ltd., USA) diluted in 1x Dulbecco's Phosphate-Buffered saline (DPBS) containing Ca^{2+} and Mg^{2+} (Gibco, Thermo Fisher Scientific). Cells on culture inserts were subjected to immunofluorescence (IF) staining or EMT induction, well plates to RNA interference (RNAi) and coverslips to ExM. Cells were incubated at 37ºC and 5.0% CO_2 and the growth media were changed three times a week. Growth media contained KnockOut™ Dulbecco's modified Eagle's medium (KO-DMEM) supplemented with 15% KnockOut™ SR XenoFree CTS™ (XF-KO-SR), 1% MEM non-essential amino acids, 2 mM GlutaMAX™, 0.1 mM β-mercaptoethanol, and 50 U/ml penicillin-streptomycin (all from Gibco, Thermo Fisher Scientific).

4.2 RNA interference

The *CLDN19* gene expression was knocked down using a commercial small interfering RNA (siRNA) kit (OriGene Technologies Inc., USA). It contained three distinct siRNA duplexes against *CLDN19*, each duplex being against different splicing variants of *CLDN19* gene product. The reference sequences of the variants can be found in National Center for Biotechnology Information with codes NM_001123395, NM_001185117 and NM_148960.

Trilencer-27 Fluorescent-labeled transfection control siRNA duplex, that was conjugated with TYE-563 fluorescence tag, was used in determining the siRNA intake efficacy (OriGene Technologies, SR30002). Transfections were performed with Lipofectamine RNAiMAX (Thermo Fisher Scientific) transfection reagent according to manufacturer's protocol. Briefly, fresh growth medium was changed two hours before starting the experiment to activate cells' normal metabolism. Cells were subjected to 1% XF-KO-SR and antibiotic free growth medium, as serum proteins and antibiotics tend to disrupt transfection by accumulating to cells. Three siRNA duplexes against *CLDN19* were pooled together and diluted to KO-DMEM, that did not contain serum proteins which could interfere the formation of siRNA-lipid complexes. To reduce transfection reagent's and siRNA's cytotoxic effects, the cells were incubated with siRNA for only 5 hours, washed with DPBS (Lonza Group AB, Switzerland) and subjected to regular growth medium. Cells with fluorescence control siRNA were fixed with 4% paraformaldehyde (PFA, Bio-Rad Laboratories Inc., USA) diluted in DPBS for 15 minutes in room temperature (RT), mounted with Vectashield (Vector Laboratories Inc, USA) containing 4′,6-diamidino-2-phenylindole (DAPI) and imaged with Olympus IX51 fluorescence microscope (Olympus Co, Japan) 24 hours post-transfection. Cells with siRNA against *CLDN19* were harvested using TrypLe (Gibco, Thermo Fisher Scientific) on day 3 and day 5 post-transfection. Non-treated control cells were harvested similarly on day 3. TrypLe was neutralized by adding growth medium and the cell suspensions were centrifuged in 300 × g for five minutes. The constituting cell pellets were dissolved in DPBS and stored in -80ºC.

4.3 Western blot

The cells were solubilized into commercial Radioimmunoprecipitation assay (RIPA) buffer (Thermo Fisher Scientific). The buffer was prepared by adding Complete Mini EDTA-free Protease Inhibitor Cocktail (Sigma-Aldrich) on ice. Cell pellets were suspended to 80µl prepared RIPA buffer. Samples were incubated on ice for 30 minutes, gently shaking the tubes occasionally. Sonication was performed with Bioruptor sonicator (Diagenode S.A., Belgium) twice with 30s on/30s off pulses with low intensity. Finally, the samples were centrifuged with 12000 × g for 20 minutes in 4ºC and the supernatants were transferred to fresh pre-cooled microcentrifuge tubes. Protein concentrations were measured using DC protein assay kit (Bio-Rad Laboratories) and absorbances were measured with a microplate reader (Wallac 1420 Victor2, PerkinElmer Inc., USA).

Laemmli 4x (Bio-Rad Laboratories) sample buffer was prepared by adding β-mercaptoethanol to 355mM concentration. Sample buffer was added to the samples, and incubation at 95ºC for

10 minutes was performed. Proteins were resolved using sodium dodecyl sulfate-polyacrylamide gel electrophoresis (SDS-PAGE). The contents of SDS-PAGE gels are represented in table 1. Total protein amounts loaded to lanes were 15µg and 80-90µg for primary porcine RPE and hESC-RPE, respectively. PageRuler Prestained Protein Ladder (Thermo Fisher Scientific) was used as a molecular weight marker. SDS-Page was performed with 60V for 20 minutes following 120V for 90 minutes. A semi-dry transfer from gels to polyvinylidene difluoride (PVDF) membranes was performed using Transblot Turbo transfer system (Bio-Rad Laboratories) with Mixed MW program. The membranes were blocked with 5% non-fat dry milk in Tween20 diluted in tris buffered saline (TBS) in 0.05% concentration (0.05% TBS-Tween) in RT for one hour. The membranes were immunoblotted against CL19 with mouse anti-monoclonal CL19 (R&D systems, USA) and mouse anti-monoclonal CL19 (Abnova Co., Taiwan) with 1:200 dilutions in 5% non-fat dry milk in 0.05% TBS-Tween. β-actin (Santa Cruz Biotechnology Inc., USA) staining with 1:1000 dilution was used as a housekeeping protein to normalize each sample. Primary antibodies were incubated in 4ºC overnight. The secondary antibody was mouse immunoglobulin G kappa binding protein (m-IgGκ BP) conjugated to Horseradish Peroxidase (Santa-Cruz Biotechnology). It was used in 1:500 dilution in 5% non-fat dry milk in 0.05% TBS-Tween and incubated in RT for one hour. Primary and secondary antibody solutions were washed with 0.5% TBS-Tween, 0.1% TBS-Tween and twice with 0.05% TBS-Tween with constant agitation for 5 minutes each. Immunoblots were created with ECL chemiluminescent detection reagent (ECL Prime, GE Healthcare Co., USA) and imaged with Molecular Imager ChemiDoc XRS+ (Bio-Rad Laboratories).

Table 1. Contents of the SDS-PAGE gels. The volumes are in microliters.

Reagent	12% Separating gel volumes	7.5% Stacking gel volumes
30% Acrylamide/Bis	4000	660
0.5M Tris-HCL pH 6.8	-	1250
1.5M Tris-HCL pH 8.8	2500	-
10% SDS	100	50
H20	3360	3000
TEMED	5	5
10% APS	50	25

4.4 EMT induction with TGF-β2 treatment

Cell lines Regea08/023 and Regea08/017 were in culture for 2 weeks and 4 weeks, respectively. Morphology images were taken with phase contrast light microscope (Nikon Eclipse TE2000-S, Nikon Inc., Japan) and transepithelial electrical resistance (TEER) values were measured (Millicell ERS-2 Voltohmmeter, Millipore Corp., USA) before starting the experiment. Cells were exposed to Transforming growth factor-beta 2 (TGF-β2, PeproTech Inc., USA) and time-response was tested with incubation times 6, 24 and 72 hours and dose-response was tested with concentrations of 10, 30 and 60 ng/ml. EMT state in living cells was evaluated with changes in cell morphology and TEER values. Cells were fixed and IF stained for further EMT state evaluation.

4.5 Immunofluorescence staining and imaging

Cells were fixed with 4% or 1% PFA in DPBS for 15 minutes or 20 minutes, respectively, and washed three times with DPBS. Permeabilization was performed with 0.1% Triton X-100 in DPBS for 15 minutes, followed by blocking with 3% bovine serum albumin (BSA) in DPBS for one hour in RT. The inserts were removed from insert holders with a scalpel. Primary antibodies were incubated overnight in +4ºC (Table 2). Excess primary antibodies were washed off 3x5 minutes with DPBS and secondary antibodies were incubated in RT for 1 hour (Table 3). Antibody washes were repeated. DNA marker Hoechst (Thermo Fisher Scientific) was added simultaneously with the first secondary antibody wash in 1:3000 dilution for detecting nuclei. Inserts were mounted between two cover slips (18x18mm, thickness 0,170±0,005mm, Carl Zeiss AG, Germany) using ProLong Gold Antifade Mountant (Thermo Fisher Scientific). Samples were imaged using Zeiss LSM800 laser scanning confocal microscope (LSCM, Carl Zeiss) with 63x oil immersion objective.

Table 2. Primary antibodies and dilutions used in immunofluorescence staining.

Primary antibody	Function	Origin	Manufacturer	Dilution
Claudin-19	RPE tight junction protein marker	mouse	R&D Systems	1:200
Claudin-19	RPE tight junction protein marker	mouse	Abnova	1:200
ARL13B	primary cilia marker	rabbit	Proteintech	1:1000
ZO-1	RPE marker	rabbit	Invitrogen	1:200
α-SMA	EMT marker	mouse	R&D Systems	1:400
N-Cadherin	EMT marker	mouse	Sigma-Aldrich	1:200
Vimentin	EMT marker	goat	Millipore	1:400

Table 3. Secondary antibodies and dilutions used in immunofluorescence staining.

Secondary antibody	Origin	Target	Ig-class	Manufacturer	Dilution
Alexa Fluor 488	Donkey	anti-mouse	IgG	Molecular Probes	1:200
Alexa Fluor 568	Donkey	anti-rabbit	IgG	Molecular Probes	1:200
Alexa Fluor 488	Donkey	anti-goat	IgG	Molecular Probes	1:200
Alexa Fluor 488	Donkey	anti-rabbit	IgG	Molecular Probes	1:200
Alexa Fluor 568	Donkey	anti-mouse	IgG	Molecular Probes	1:200

4.6 Expansion microscopy

ExM was performed as previously described.[57] IF staining was performed as already explained (4.5) with minor adjustments. Primary antibody dilutions for CL19 and primary cilia marker ARL13B were 1:50 and 1:500, respectively. Secondary antibody dilutions were 1:100. Both antibodies were incubated in RT for 1 hour. 6-((acrolyl)amino)hexanoic Acid Succinimidyl Ester (Acrolyl X-SE, Thermo Fisher Scientific) was used as an anchoring reagent with a concentration of 0.1 mg/ml. 300 µl of anchoring solution was added on top of each sample. Anchoring treatment was incubated in RT protected from light overnight following washing with DPBS for 2x15 minutes.

The protocol for gelation and expansion steps is illustrated in Figure 6. In-house three dimensional (3D) printed coverslip spacer (diameter 10 mm, depth 400 µm) was placed on the parafilm coated glass coverslip (Carl Zeiss). Gelling solution was prepared on ice. Gelling solution contained 94µl monomer solution (Table 4), 1.5 µl H_2O, 0.5 µl Hydroxytempo, 2 µl tetramethylethylenediamine (TEMED) and 2 µl ammonium persulfate (APS). 70 µl of gelling solution was added to the spacer. Coverslip that had the cells attached to it was placed on top of the spacer, cells towards the gelling solution. Samples were left in RT for 45 minutes to polymerize. After polymerization, the parafilm coated coverslip and the spacer were removed, and the gel attached to the sample coverslip was placed to a fresh well plate. The gel was measured to know the original gel diameter before the expansion. Digestion solution contained 50 mM Tris pH 8.0, 1 mM ethylenediaminetetraacetic acid (EDTA), 0.5% Triton X-100 and 0.8 M guanidine HCL. Prior to use, proteinase K was added to the digestion solution to a final concentration of 8 units/ml. Digestion solution was added to the gel and incubation in RT protected from light was performed overnight. After digestion, the gel was moved to a 6-cm dish for expansion steps. The gel was washed 5x1 hour with an excess volume of H_2O. During the expansion, the coverslip detached from the gel. After the expansion, the gel diameter was measured, and the expansion factor was calculated according to the equation:

$$Expansion\ Factor = \frac{Diameter\ after\ expansion}{Diameter\ before\ expansion}$$

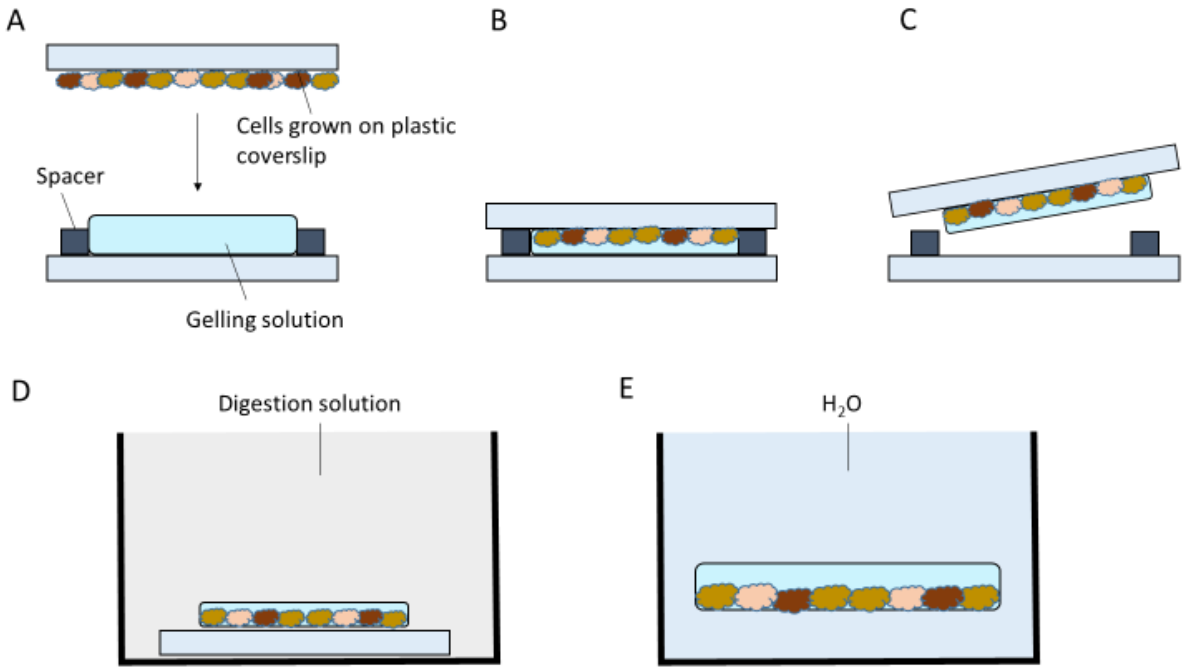

Figure 6. Schematic representation of gelation and expansion steps. A) A sideview of the gelation chamber. The spacer is attached to a parafilm coated coverslip and gelling solution is added to the spacer. Cells grown on a coverslip are placed on top of the chamber. B) The gel is left to polymerize in RT for 45 minutes. C) A schematic showing that after polymerization the gel is attached to cells. The parafilm coating of the bottom coverslip prevents the gel from sticking to it. D) The gel is placed to digestion buffer and left to incubate in RT overnight. The gel with cells is still attached to the coverslip. E) After digestion the gel is moved to another dish and incubated with excess water for 5x1 hour until the expansion reaches plateau. The coverslip detaches from the gel during the expansion.

Table 4. Components of the monomer solution. The concentrations are in g/ml (except DPBS) and the amounts are in microliters.

Component	Stock concentration	Volume	Final concentration
Sodium Acrylate	0.38	2250	0.086
Acrylamide	0.4 (40%)	580	0.025
N,N'-Methylenebisacrylamide	0.02 (2%)	750	0.0015
Sodium chloride	0.292	4000	0.117
DPBS	10x	1000	1x
H_2O		820	

The gel was prepared for imaging to live-cell imaging chamber (Aireka Scientific Co. Ltd., China). A round piece of the gel was cut by using an in-house 3D-printed holder with a diameter

of 14 mm. The gel was transferred to the imaging chamber, cells downwards, and the holder was placed around the gel. 13 mm coverslip was placed on top of the gel and low-melt agarose was heated and added inside and outside the holder to keep the set-up stable. Samples were imaged with Nikon A1R microscope using water immersion 60x objective.

4.7 Image data-analysis

Image processing of confocal images from LSCM and ExM was performed with ImageJ.[58] Only brightness and contrast were adjusted for LSCM images. In addition, deconvolution was performed to the images from ExM with Huygen Essential Deconvolution Wizard. Image properties were adjusted so that the pixel sizes were divided with the expansion factor to convert scale bars that were in correlation with the expanded cells.

Maximum intensity projections (MIP) of ARL13B marker images were converted and primary cilia lengths were calculated with ImageJ (Figure 7). Before skeletonization, narrow primary cilia had to be thickened to prevent skeletonization from cutting the cilium. Maximum Branch Lengths were exported from the resulting table and these lengths were collected into Excel and imported to R as a CSV file.

```
run("Adjust", "Threshold…" "B&W", "Dark background")
run("Process", "Binary", "Skeletonize")
run("Analyze", "Skeleton", "Skeleton 2D/3D")
```

Figure 7. The imageJ commands to measure primary cilia lengths.

4.8 Data-analysis

Normality of the data was tested using Shapiro-Wilk normality test. As the cilia lengths were not normally distributed in either of the groups, Mann Whitney U test was performed to test whether primary cilia lengths differed between groups. A p-value less than 0.05 was considered significant. All the tests were performed with R version 3.6.0.

5 Results

5.1 RNA interference failed to knock down *CLDN-19* expression

5.1.1 RNA interference and Western blot optimizations

Before starting RNAi studies, the transfection reagent's transfection efficiency was tested with siRNA tagged with a fluorophore TYE-563 and hESC-RPE cells cultured 24 hours after plating. Cells were fixed, mounted and imaged to evaluate the siRNA intake efficacy (Figure 8). The test showed Lipofectamine RNAiMAX to be functioning in transfecting hESC-RPE cells with 73% (n=590 cells, calculated from 1 image) siRNA intake based on one experiment. Furthermore, several parameters were optimized (Table 5).

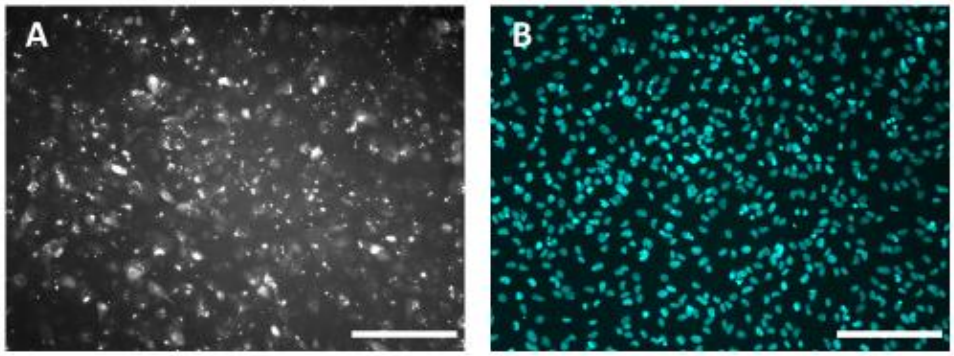

Figure 8. siRNA intake evaluation. Transfection of fluorophore tagged siRNA (10nM) with Lipofectamine RNAiMAX transfection reagent was tested on hESC-RPE cells 24 hours after plating. A) Fluorescence control. The siRNA intake was 73% (n=590). B) Nuclei stained with DAPI marker. Scale bars 200µm.

Table 5. RNAi protocol optimization. Data not shown. Transfection reagent incubation time and transfection medium were important parameters to be optimized.

Parameter	Method	Outcome
siRNA and Lipofectamine incubation time	72h	Cell deaths, wide areas without intact cells
	5h	No cell death, remained confluent
Cells cultured before WB	2 days	Harvest day did not alter the protein levels in WB
	3 days	
	5 days	
Transfection medium	Regular growth medium	Poor siRNA intake by visual evaluation
	Modified medium (1% XF-KO-SR, no antibiotics)	Increased siRNA intake by visual evaluation
siRNA concentration	10nM	Did not affect protein levels in WB, best siRNA intake by visual evaluation with 30nM
	30nM	
	50nM	

WB optimizations were performed with primary RPE extracted from porcine eyes. Throughout optimizations, the resulting CL19 band was around 40 kDa (Figure 9) whereas its calculated molecular mass is approximately 23 kDa based on the amino acid sequence (https://www.uniprot.org/uniprot/Q8N6F1:28.1.2020). The resulting 40kDa band could have possibly been a dimer of CL19, as claudin proteins have previously been detected from tissue samples in WB.[59] However, this issue was not further studied in this project. Furthermore, several parameters were optimized (Table 6). As siRNA transfection and WB protocols were optimized, RNAi studies were started.

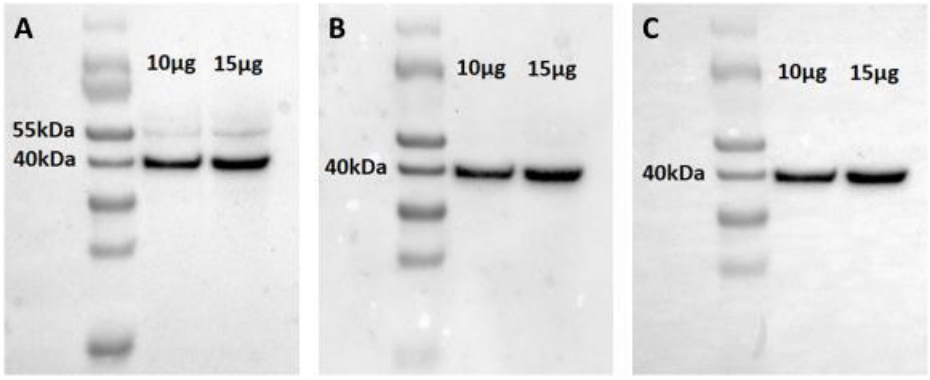

Figure 9. Western blot optimization with porcine RPE cells. WB protocol was optimized with primary RPE cells from porcine eyes with two CL19 antibodies from different manufacturers and β-actin as a loading control. 10 or 15µg of total protein extract was loaded per lane. A) WB stained against CL19 (R&D Systems). B) WB stained against CL19 (Abnova). C) WB stained against β-actin.

Table 6. Western blot optimization. The most notable difference was brought by optimizing total protein amounts per lane.

Parameter	Method	Outcome	Chosen method
Lysis buffer	Laemmli 2x	Good lysis, not compatible with protein assay	
	Laemmli 4x	Really thick solvent, hard to handle	
	Additional buffer*	Excellent lysis of the cell pellet	
	RIPA	Good lysis	RIPA
Boiling	95°C 10 min	Different boiling procedures did not affect the band sizes or migration	95°C 10 min
	95°C 5 min		
	70°C 5 min		
	37°C 10 min + 95°C 5 min		
	40°C 30 min		
	RT 45 min		
Protein amount per lane			
primary porcine RPE	10 µg	Clear band	
	15 µg	Clear band	
	50 µg	Smeared band	15 µg
hESC-RPE	30 µg	No band	
	70 µg	Faint band	
	80 µg	Good band	
	90 µg	Good band	
	110 µg	Dark lanes	80-90 µg
Denaturing environment	Laemmli (b-metOH)	Different reducing agents did not dissolve 40kDa band to 23kDa.	Laemmli (b-metOH)
	Novex (EDTA, DTT)		
	Laemmli (b-metOH + Urea)		
Sonication	Low voltage, 30 s on 30 s off, 1 pulse	Strong band, more protein extracted from cells	Low voltage, 30 s on 30 s off, 1 pulse
	No sonication	Fainter band	
Antibody dilutions			
CL19 (R&D Systems and Abnova)	1:1000	Faint band	
	1:500	Faint band	
	1:200	Good band	1:200
m-IgGkappa BP-HRP	1:1000	Nothing detected	
	1:500	Good band detection	1:500

*Additional buffer contained 50nM HEPES and 150mM NaCl supplemented with 1% Triton x-100, 1xEDTA, 1xproteinase inhibitor

5.1.2 RNA interference experiments

RNAi experiments were performed on hESC-RPE cells cultured for 14 days to ensure monolayer confluency. Confluency increased CL19 levels, and higher CL19 amount ensured detection in WB. Nevertheless, the transfection optimization 24 hours after plating was performed to confirm that hESC-RPE cells can be transfected with this transfection reagent, as RPE cells more easily intake molecules while they are still proliferating. Further optimization steps would have been required to optimize the transfection in day 14 time point. Transfection reagent with fluorescence control siRNA were incubated for 5 hours, washed off and siRNA intake was evaluated 24 hours post-transfection (Figure 10 A, B). The siRNA intake was poor as only few cells were transfected. Transfection reagent with siRNA against *CLDN19* was incubated for 5 hours, washed off and cells were harvested 3- or 5-days post-transfection. The fluorescence control and siRNA against *CLDN19* were not incubated similarly, as the manufacturer advised that the fluorescence control had to be evaluated no later than 24 hours post-transfection. In addition, CL19 siRNA incubation must be days rather than hours, to ensure protein level decreasing by protein turnover, when the CL19 expression is knocked down. Protein samples were extracted and subjected to WB (Figure 10 C, D, E). RNAi had no effect on CL19 protein levels as indicated with relative signal intensities normalized to β-actin. As RNAi failed to produce CL19 knockdown cells, physical changes of primary cilia were not examined.

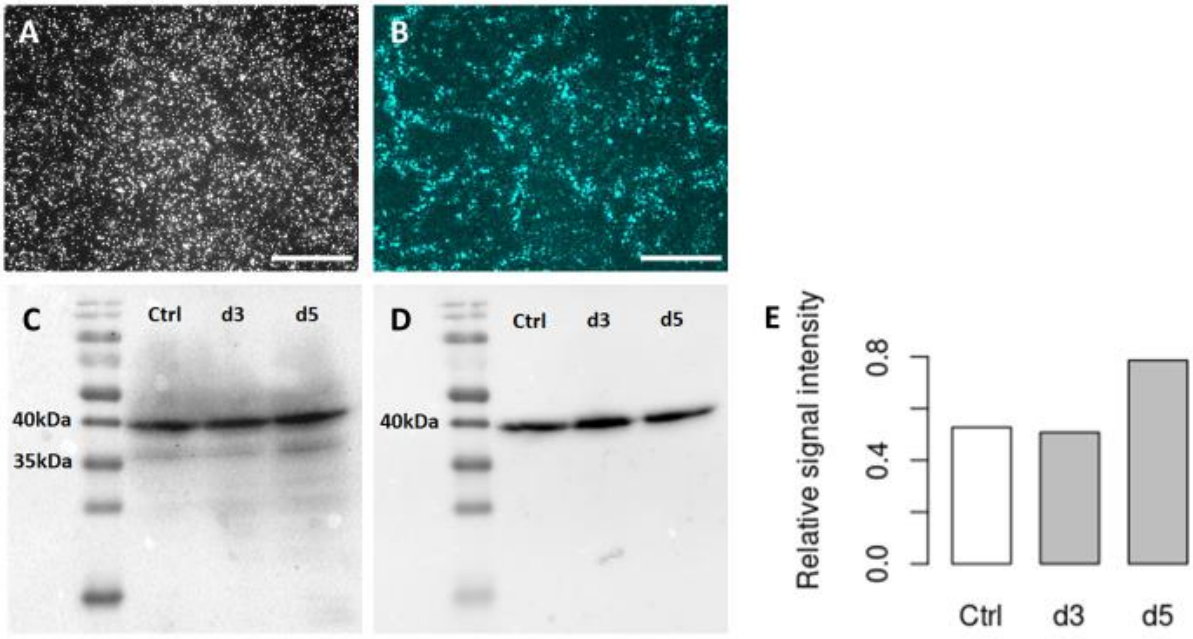

Figure 10. RNA interference failed to decrease CL19 protein level. A) Fluorescence control image. TYE-653 fluorophore got presumably caught to the cell membrane which can be seen as bright aggregates. The transfected cells in the image are much fainter. B) Nuclei stained with DAPI. C) WB stained against CL19. D) WB stained against β-Actin. E) Quantification of CL19 band intensities between samples (n=1). Intensities are normalized against β-actin band intensities. d5 bar is relatively higher than others, which indicates higher CL19 protein level in that sample. Scale bars 200 µm.

5.2 Paraformaldehyde concentration and expansion microscopy optimizations

CL19's localization in primary cilia was studied to find a connection between the protein and primary cilia and ultimately the reason, why this ciliary localization of CL19 is only occasional. PFA concentrations 1% and 4% in DPBS were tested to enhance antibody specificity on tight junctions. CL19 antibodies reached the target protein better when excess crosslinking is not blocking the epitopes (Figure 11). Fixation with 4% PFA led to ruptures of the epithelium while expanding the gel during ExM, whereas 1% PFA did not lead to similar rupturing effects (data not shown, n=3). Therefore, 1% PFA was preferred as fixative throughout this study in IF staining when possible and in ExM. Furthermore, ExM permitted efficient resolution in confocal images (Figure 12). The ARL13B localization was comparable with our previous structured illumination microscopy images of primary cilia (unpublished data) and with a previous study about ciliary proteins by Kohli and colleagues.[60] Therefore, the ExM was confirmed to be reliable method to study CL19 localization in primary cilia. EMT inductions were performed to study if it could direct CL19 to localize in primary cilia. It was also used to find the precise localization site of CL19 within primary cilia.

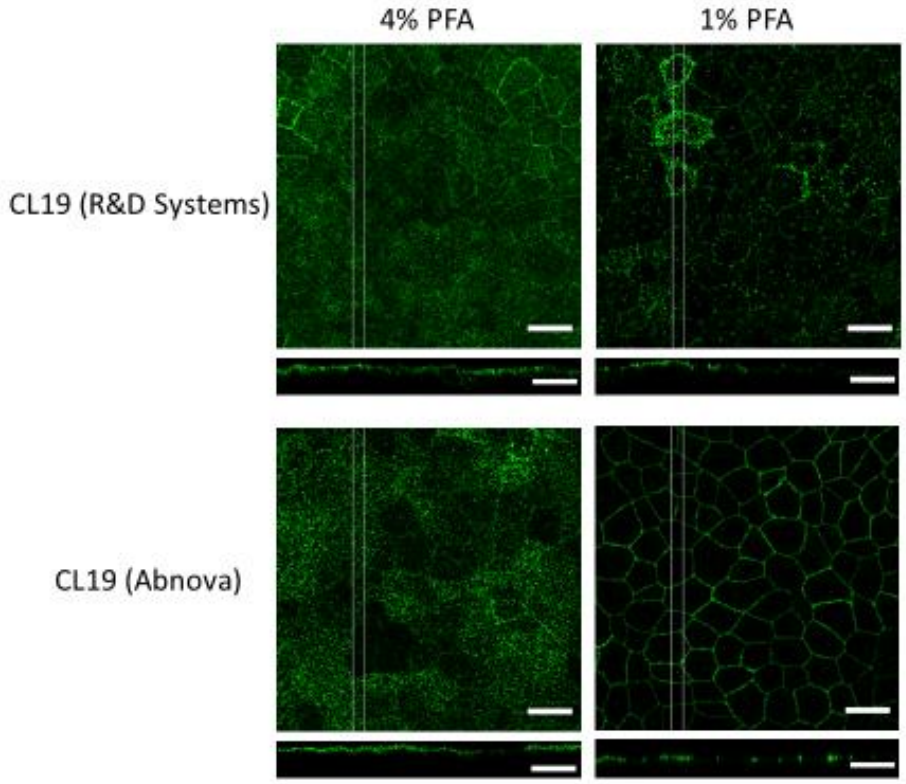

Figure 11. MIP images of PFA concentration optimization in IF staining. PFA concentrations 4% and 1% were compared with two CL19 antibodies from different manufacturers. With 4% PFA, staining is diffuse as the CL19 antibody binds non-specifically. Using 1% PFA enhances CL19 antibody binding specificity. Cells cultured 5 weeks after plating. Scale bars 15µm.

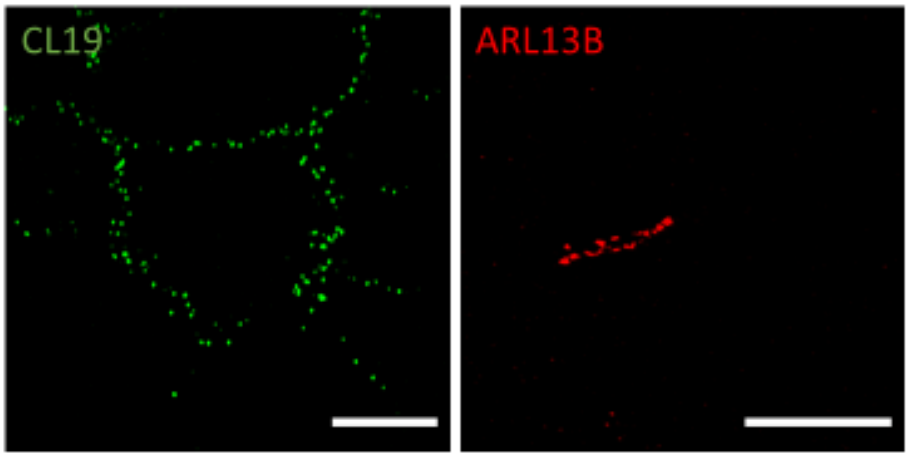

Figure 12. Expansion microscopy MIP images. CL19 (R&D Systems) is localized to tight junctions and is seen as beaded-necklace arrays. ARL13B is showing a single primary cilium. Scale bars 5µm.

5.3 EMT induction with TGF-β2

Previous studies have indicated that TGF-β treatment is effective in inducing EMT in human fetal PRE (hf-RPE) and Adult Retinal Pigment Epithelial cell line-19 (ARPE-19) cell lines.[61-63] Our previous data has indicated that poorly differentiated, rather fusiform cells possess long primary cilia with CL19 localizing to it (unpublished data). Therefore, hESC-RPE cells (Regea08/023) were subjected to EMT induction two weeks after plating using TGF-β2 treatment with different concentrations and exposure times. During TGF-β2 treatment, the EMT progression was evaluated with changes in cell morphologies and TEER values. However, at 2 weeks already prior the TGF-β2 treatment, cells were unmatured and unpigmented and as result not visible with phase-contrast microscope. In addition, TEER values under $50\Omega*cm^2$ are considered low, whereas RPE that has a TEER value over $200\Omega*cm^2$ is considered a tight epithelium.[12] Therefore, the average TEER value before starting the experiment, $31\Omega*cm^2 \pm 3\Omega*cm^2$ (mean ± standard deviation, n=16), was relatively low. The TEER value changes were normalized against non-treated control and the percentual changes were plotted into a bar plot (Figure 13). Slight decrease of TEER values was detected based on the bar plot. Nevertheless, the starting TEER values were relatively low, indicating that there the epithelium is not intact. Therefore, the detected changes were not reliable and statistical testing to confirm differences between groups was not performed. Therefore, EMT state had to be evaluated merely based on the IF staining. Cells were immunolabeled against tight junction marker ZO-1 and EMT marker Alpha-smooth muscle actin (α-SMA) to evaluate the EMT state (Figure 14). Both markers show that cells had turned to more fusiform morphology. ZO-1 intensity was decreased, and the morphology of the junctions had changed in both concentrations. Simultaneously, α-SMA expression is upregulated with both concentrations. In addition, the nuclei with TGF-β2 treated cells have taken more elongated morphology. Immunostainings were also performed against CL19 and ARL13B to see whether EMT induces ciliary length and CL19 localization to primary cilia (Figure 15). It was noted that these cells produced very few primary cilia and CL19 is faint and not localized to tight junctions. Together with the fact that TEER values were relatively low, it was thought that the cells did not produce good enough RPE and the EMT testing was repeated with another cell line Regea08/017. In addition, the cells were cultured 4 weeks to make sure that the cells were mature enough for normal CL19 localization and to produce primary cilia.

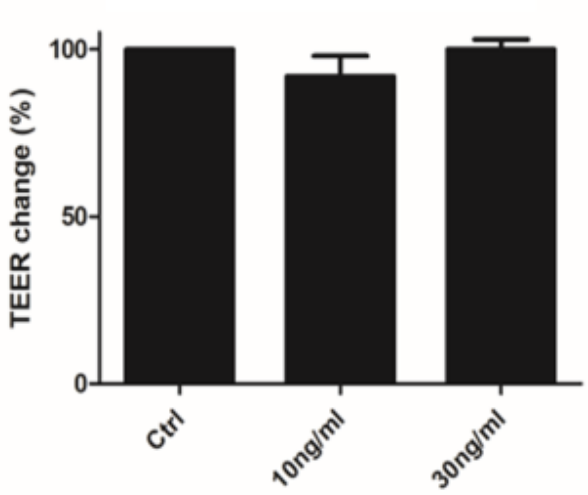

Figure 13. Changes in Regea08/023 RPE TEER values due to the TGF-β2 treatment. The TEER value changes are normalized against non-treated control. The error bars show standard deviation.

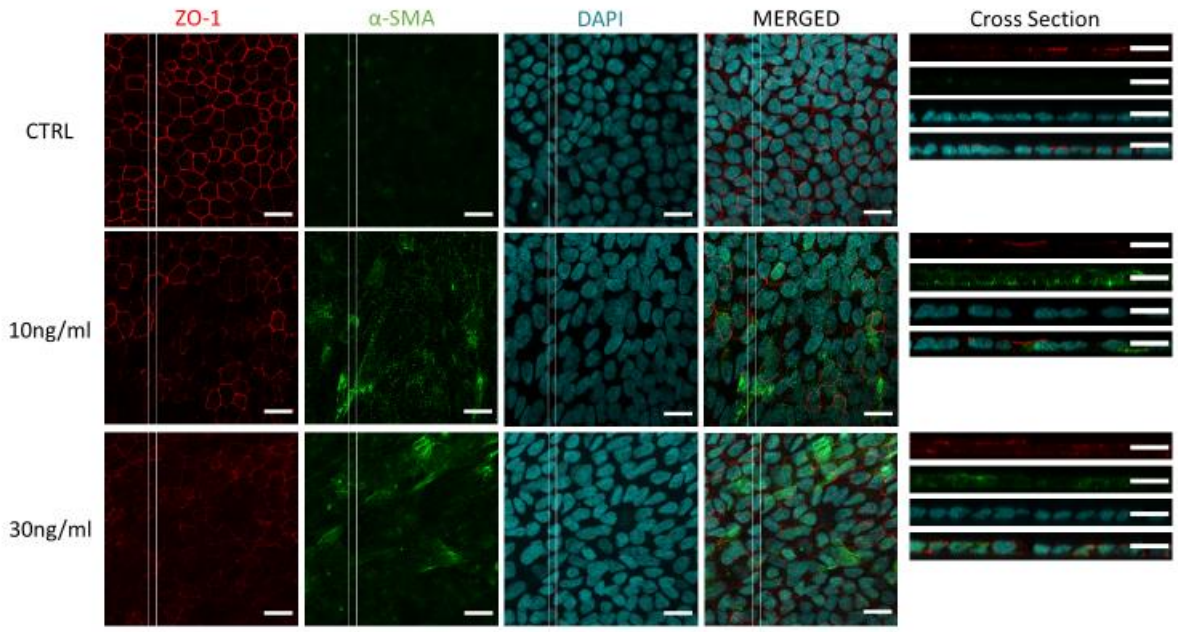

Figure 14. MIP images of EMT state evaluation IF staining for cell line Regea08/023. Non-treated hESC-RPE as a control and hESC-RPE treated with 10 or 30ng/ml TGF-β2 for 24 hours. Cells are stained against ZO-1, αSMA and DAPI. Scale bars 15µm.

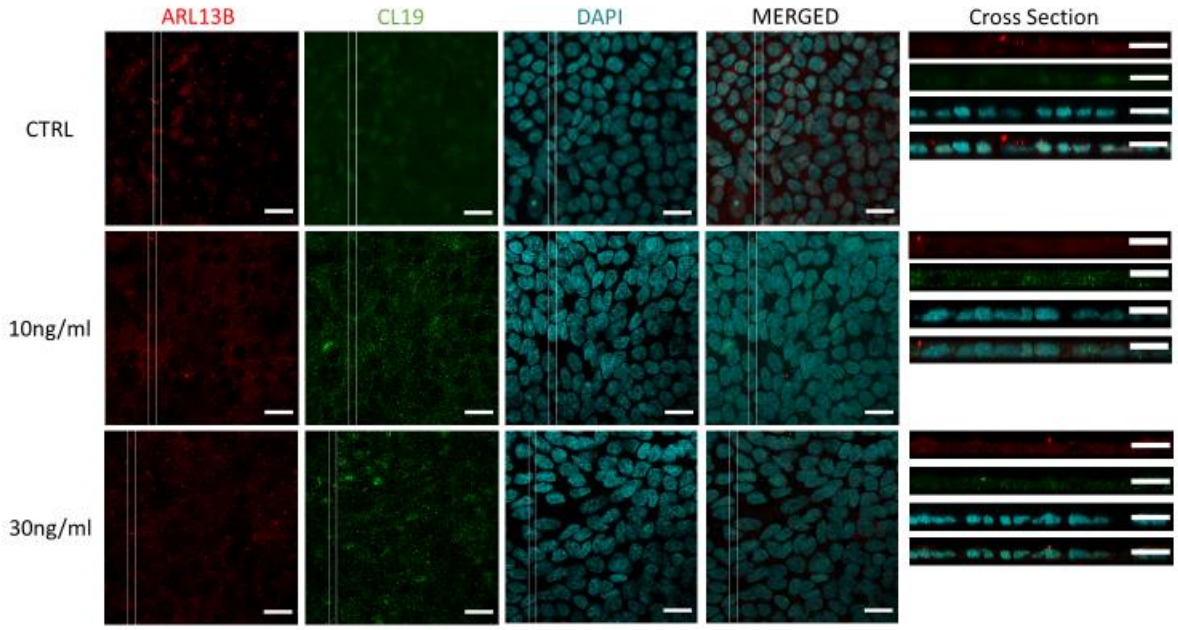

Figure 15. MIP images of ciliary responses to EMT in cell line Regea08/023. Non-treated hESC-RPE as a control and hESC-RPE treated with 10 or 30ng/ml TGF-β2 for 24 hours. Cells are stained against ARL13B, CL19 and DAPI. Scale bars 15µm.

Regea08/017 hESC-RPE cells subjected to EMT induction were visible with phase-contrast microscope (Figure 16) due to pigmentation which indicated higher maturation state than with the Regea08/023 cell line. Surprisingly, there were some fusiform cells disrupting the RPE monolayer. This explains why the TEER values remained relatively low, $43\Omega*cm^2 \pm 12\Omega*cm^2$ (n=16), also with this cell line despite they were cultured for four weeks. The TEER value changes were normalized against non-treated control and the percentual changes were plotted into a bar plot (Figure 17). The possible change seen in the TEER values were stated nonsignificant, as the RPE was not intact before starting the experiment.

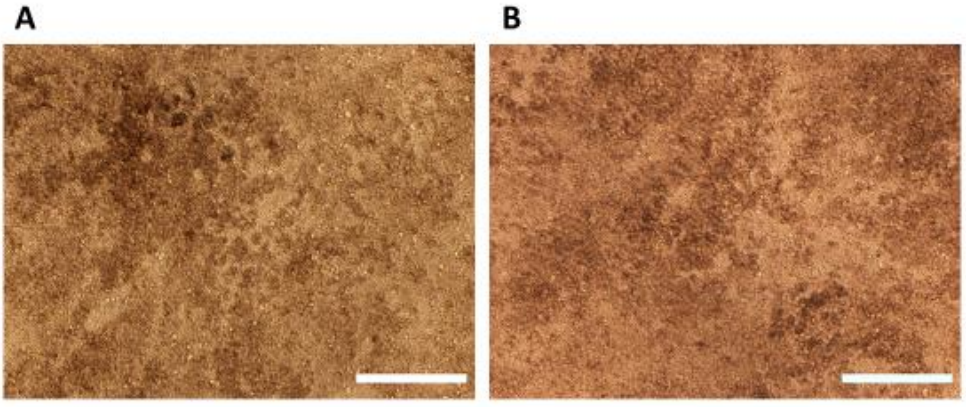

Figure 16. Phase-contrast images representing hESC-RPE morphology. A) hESC-RPE layer before starting the TGF-β2 treatment. B) hESC-RPE monolayer treated with 30ng/ml TGF-β2 for 24 hours. Scale bars 200µm.

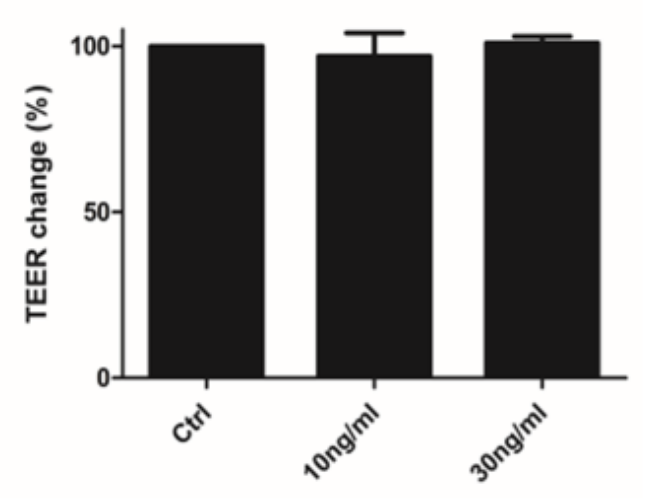

Figure 17. Changes in Regea08/017 RPE TEER values due to the TGF-β2 treatment. The TEER value changes are normalized against non-treated control. The error bars show standard deviation.

With Regea08/017 cell line, ZO-1 and α-SMA were down- and upregulated, respectively, similarly as with the Regrea08/023 (Figure 18). This cell line produced primary cilia with prevalence typically observed with these cells (unpublished data, Figure 19). Nuclei were again elongated, indicating that the EMT causes the cells to become more fibrotic. Interestingly, cells treated with 30ng/ml TGF-β2 show CL19 and ARL13B colocalization, which was observed in more detail (Figure 20). Primary cilia lengths were measured and resulted data is shown in box plots (Figure 21). Shapiro-Wilk test of normality was performed to see whether the cilia lengths are normally distributed among control, 10ng/ml and 30ng/ml samples. The p-values from this test were $1.5x10^{-11}$, $1.5x10^{-4}$ and $2.2x10^{-16}$, respectively. Thus, null hypothesis of data normality was rejected, and a nonparametric statistical test was chosen for further testing. Mann-Whitney U test was performed between control and 10ng/ml sample and control and 30ng/ml sample. The medians of primary cilia lengths were 0.80µm, 0.93µm and 0.81µm for control, 10ng/ml treated and 30ng/ml treated groups, respectively. The difference between primary cilia lengths against control group was not significant for 10ng/ml (p-value=0.19) or 30ng/ml (p-value=0.92). Thus, there were no statistically significant differences in primary cilia lengths between groups, even though there were more of elongated primary cilia with the higher concentration of TGF-β2. It is possible that the primary cilia counts were too little to get significant differences. However, this study suggests that EMT state directs CL19 to primary cilia.

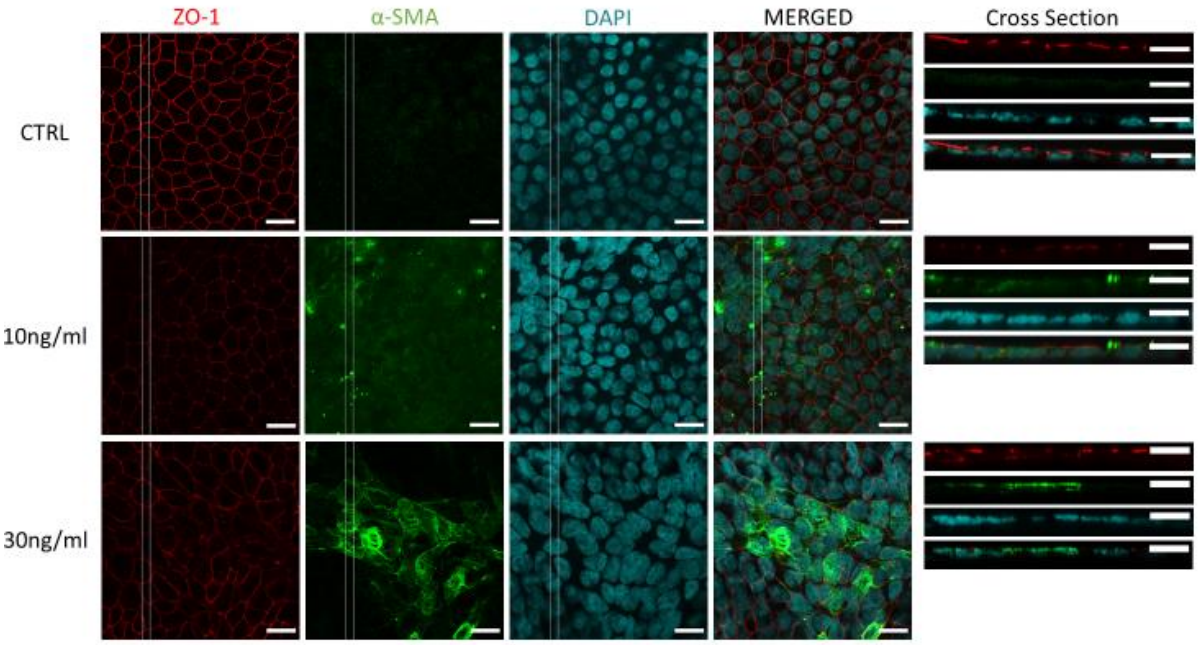

Figure 18. MIP images of EMT state evaluation IF staining for cell line Regea08/017. Non-treated hESC-RPE as a control and hESC-RPE treated with 10 or 30ng/ml TGF-β2 for 24 hours. Cells are stained against ZO-1, αSMA and DAPI. Scale bars 15µm.

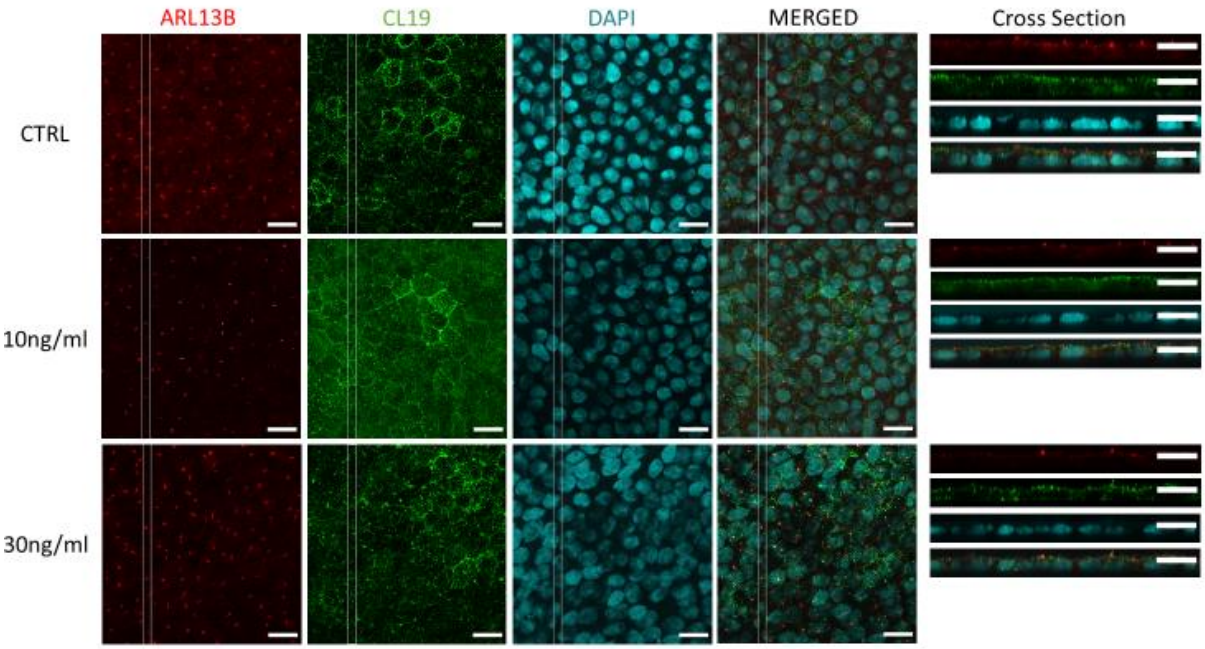

Figure 19. MIP images of ciliary responses to EMT in cell line Regea08/017. Non-treated hESC-RPE as a control and hESC-RPE treated with 10 or 30ng/ml TGF-β2 for 24 hours. Cells are stained against ARL13B, CL19 and DAPI. Scale bars 15µm.

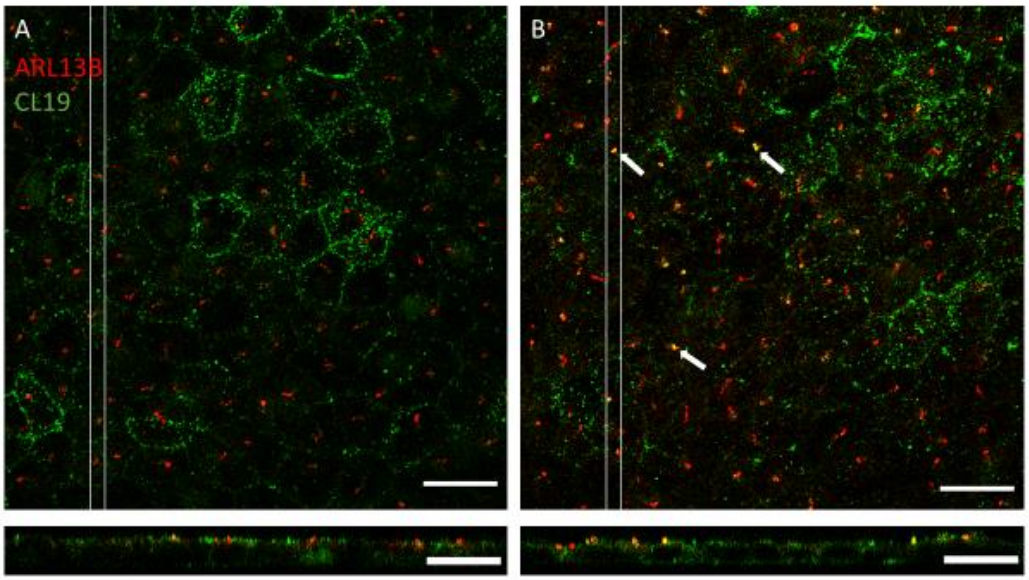

Figure 20. Comparison of CL19 protein's ciliary localization. A) Control cells do not possess CL19 immunopositive primary cilia. B) Cells treated with 30ng/ml TGF-β2 for 24 hours produce multiple CL19 immunopositive primary cilia, shown as yellow color indicating colocalization of CL19 and ARL13B. White arrows indicate few CL19 immunopositive primary cilia. These are visible also in the cross-section image under the overlay image. All images are MIP. Scale bars 15µm.

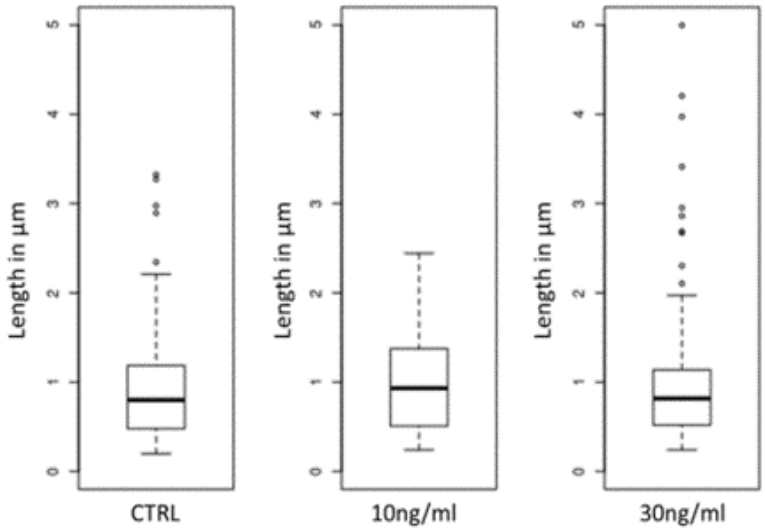

Figure 21. Primary cilia lengths. Boxplots represent ciliary lengths in control sample, 10ng/ml and 30ng/ml TGF-β 24 hours treated samples. Medians for each group were 0.80µm, 0.93µm and 0.81µm respectively. The data was from 1 experiment and analyzed primary cilia counts for control, 10ng/ml and 30ng/ml were 220, 115 and 209, respectively.

6 Discussion

The aims of this thesis project were to study the role of CL19 in hESC-RPE primary cilia maintenance, EMT's effect on CL19 localization in primary cilia and the localization site of CL19 in primary cilia. RNAi was selected to knock down the expression of CL19 because of its low cost and simplicity to use. It has also been used by others, which gave insights to optimizations. WB was used in assessing RNAi efficacy. Quantitative polymerase chain reaction could have been used in this intention to detect changes in RNA levels. It would have been more suitable as quantitative analysis as WB is producing only relative quantities of the proteins. However, in this study it was crucial that the RNAi affects directly to the protein levels, in order to find reliable physical effects in cells in response to decreased CL19 concentration. RNA concentration does not always correspond to protein levels in given time point; thus, WB was chosen to observe RNAi efficacy in this study. The microscopy methods that were used were LSCM and ExM. The cells were subjected to EMT using TGF-β2 treatment. TGF-β2 was chosen because it has been used by others, its low cost and efficacy.

6.1 Detected claudin-19 band with Western Blot was bigger than expected

The WB was optimized with primary RPE cells that were derived from porcine eyes. Several different approaches were tested in cell lysis and denaturing of the protein solution. The major difference was accomplished with reducing the protein mixture amount in SDS-PAGE wells. In primary RPE cells the amount of CL19 is enormous compared to RPE cells cultured *in vitro*. Cultured cells will probably never reach the same level of maturity that is observed in primary RPE cells. Therefore, the total amount of protein solvent from hESC-RPE cultured *in vitro* was over 5 times greater than required from primary RPE cells. The RIPA buffer was shown to be most promising among other lysis buffers. Laemmli sample buffer was efficient in lysing the cells, but due to its' strong color, it is not compatible with protein concentration assays. Additional lysis buffer tested was efficient in lysing the cells. It immediately dissolved the cell pellet after adding the buffer, whereas in other buffers the cell pellet had to be physically dissolved by pipetting. Nevertheless, the commercial RIPA buffer was simpler to use, as it did not require preparation. Therefore, RIPA buffer was selected to be used in later parts of the study. Adding sonication to the protocol seemed to increase the overall protein yield based on DC assay results. Supposedly, the sound beams of sonication break the cell membranes even further and more protein is dissolved into the protein solution. Therefore, sonication became a part of the standard extraction protocol.

Membrane proteins can have properties that affect SDS-PAGE in a way that they do not dissolve normally as highly hydrophobic proteins tend to form aggregates in high temperatures.[64,65] A crucial step to be considered was whether to boil the samples during denaturation or not. Thus, different boiling temperatures for CL19 detection with WB were tested. However, the boiling did not seem to cause CL19 aggregate formation. CL19 has only four transmembrane domains[66,67], therefore it can be assumed that the hydrophobic properties of the protein are so minor that high temperatures do not cause aggregate formation. Thus, the samples were boiled after adding sample buffer to strengthen the denaturing effects. During the experiments, it became evident that freezing the protein lysate before SDS-PAGE had effect on the CL19 detection from the PVDF membrane. When protein lysate was directed straight to SDS-PAGE after the lysis, the CL19 bands in the membrane were clear and there was not any nonspecific binding of antibodies. When the samples were frozen and thawed before SDS-PAGE, the constituting images of the blots were bad quality. They were dark and had a lot of nonspecific binding and CL19 antibody from Abnova even failed to detect the CL19 bands. This leads to the idea that perhaps the hydrophobic proteins' conformation is affected after freeze-thaw cycle and they do not dissolve normally in SDS-PAGE. This cycle could also break the protein so that it cannot be detected in WB. Therefore, it should be preferred to subject membrane protein samples to SDS-PAGE straight after cell lysis.

An interesting issue that arose during WB experiments was the size of the detected CL19 band. The detected band repeatedly was the size of 40kDa, whereas according to the literature, the CL19 monomer is only 23kDa.[37] WB is not ideal in protein mass determination. In principal, the migration is based solely on the mass of the protein as 3D structure is reduced and charge is controlled by SDS molecules.[68] However, different post-translational modifications (PTM) affect the expected band sizes. The reference mass 23.229 kDa from UniProt is determined by estimating based on amino acid sequence. Thus, it does not consider the PTMs. Claudin proteins are reported to have at least phosphorylations, palmitoylations, glycosylations and ubiquitinations.[28,30] However, in PTM database PhosphoSitePlus® (v.6.5.8) there are only three phosphorylations reported for CL19. One phosphorylation to a molecule adds around 80Da to its molecular weight.[69] Thus, the actual mass change from three phosphorylations in CL19 cannot entirely explain the difference between observed and predicted band size. Nevertheless, even one phosphorylation can have drastic effect in detected molecular weight in WB, because it can change the mass-charge expectations. In addition, proteins that have multiple positive amino acid residues in their sequence tend to migrate slower than expected based on their

mass.[68] For example, it is shown how REDD1 protein migrates around 35kDa on WB, even though its' predicted molecular mass is around 25kDa. This is said to be because of its multiple positive lysine residues.[70] According to UniProt, REDD1 has 6/232 lysines in its sequence whereas CL19 6/224 lysine residues. This could explain the slower migration than expected for CL19.

One reasonable explanation to this relatively slow migration could be that the protein has a dimeric conformation. Based on a previously published protocol, the claudin proteins can be detected as dimers in WB, especially while extracted from tissue samples.[59] There are not too many studies on CL19 protein properties that could help in speculating the challenges in WB in this study. For example, the half-time or conformation in RPE are not reported for CL19. The crystallography conformations for different claudin proteins were determined in a previous study by Irudayanathan and colleagues.[71] For CL19, it was stated that it forms dimers or even trimers with CL16 in kidney. It has also been studied whether the monomers of emerging CL19 homodimers are produced by two adjacent cells or are they produced by a single cell.[6] Thus, it is reasonable to speculate that the detected band of 40kDa could be a dimer form of CL19. Nevertheless, the denaturing environment before SDS-PAGE is powerful. Different denaturing conditions were tested with B-mercaptoethanol and dithiothreitol (DTT), and they both resulted with the same band size. Therefore, it could be hypothesized that after denaturation, the monomers could renature back to the original dimeric conformation. This was studied by adding EDTA to prevent renaturation from happening as was done in a previous study.[2] Nevertheless, it did not have an effect and the band size remained 40kDa.

The nature of antibodies should also be considered in this situation. Two different antibodies were tested in WB against CL19. They both are also used in IF; therefore, they bind the protein when it is in 3D conformation in tight junctions. Either of the antibody manufacturers do not report the target sequence of the antibodies. Thus, it cannot be verified, whether these antibodies require specific 3D-structure in order to detect the protein. There is a slight possibility that these antibodies are not able to bind CL19 protein monomer. This could happen when the antibody does not recognize the required structure that forms when two monomers combine into a dimer. Nevertheless, the antibody from Abnova is particularly manufactured to WB analysis, thus it should be able to bind also the monomer structure of CL19. All in all, the most reasonable explanation to surprising molecular mass is the differing charge-mass ratio due to positively charged residues and phosphorylations.

It should be ensured that the detected band reliably was CL19. ARPE-19 cell line could have been used in this manner, as it does not express CL19.[72] Another approach could have been using a significant blocking peptide.[73] Blocking peptides are used by first performing WB and antibody stripping in a conventional manner and detecting the suspected CL19 band. After stripping, the blot is treated with blocking peptide that binds to CL19, after which the antibody treatments are repeated. If this approach fades the suspected CL19 band, it can be confirmed that it surely is CL19 and not nonspecific binding of antibodies. Nevertheless, the WB experiments repeatedly resulted with 40kDa band with cells from different sources and with different antibodies. More optimization steps about this issue can be performed in the future, but in this study the RNAi experiments were performed with the assumption that the 40kDa band was CL19.

6.2 Transfections led to poor siRNA intake

The transfection reagent Lipofectamine RNAiMAX was shown to be efficient in transfecting RPE cells that were plated one day before the transfection and 90% confluent. This time point would have been optimal to study early stages of ciliogenesis as it begins soon after confluency is reached, and the cell division machinery is shut down.[74] To study CL19's role in ciliogenesis would have probably been straightforward. If the role of CL19 was in ciliogenesis, the knock down would lead to absence or shortening of primary cilia, which is relatively easy to verify with microscopy. Nevertheless, the production of CL19 on protein level can be observed only after certain time since the cells have reached confluency. Therefore, the focus of this study was to investigate, if CL19 knockdown would affect primary cilia maintenance and the cells were cultured 14 days, before starting the RNAi experiments. Nevertheless, RPE cells are relatively difficult to transfect. The uptake of fluorescence labeled siRNA was deficient with cells that had been 14 days in culture. The transfections were performed three times with different set ups but only few cells showed fluorescence. 30nM siRNA was most efficient based on fluorescence control siRNA intake. However, it was performed only once, and it cannot be stated whether this slight increase in fluorescence control siRNA intake was because of the siRNA concentration rather than other adjustments in the experiment.

It is impossible to conclude on why the transfection was inefficient. There was time for only few repetitions and many promising adjustments in the protocol were not tested. While starting a RNAi study with cells that are hard to transfect, it could be useful to confirm that the protocol is otherwise functional with a cell line that is easy to transfect.[75] It should be a cell type that expresses CL19 and is easy to transfect in order to test the whole protocol with all reagents and

components. The problem is that presumably all CL19 expressing cells are robust and therefore hard to transfect. If the protocol can be proved efficient, the major pitfall of siRNA intake must be solved. In a previous study, CL19 knockdown in hf-RPE was established with parallel transfections on day 1 and 3.[2] Nevertheless, it must be noticed that hf-RPE cells are not as robust as our hESC-RPE cells. In addition, hESC-RPE cells in different confluency stages were successfully transfected with RNA using Stemfect transfection reagent (Stemgent Inc., USA). Even cells cultured for 28 days showed great transfection efficacy.[75] These results seem promising, even though the RNA used was mRNA and not siRNA. The manufacturer states that the reagent can be used also with siRNA (Stemgent, 00-069), therefore this reagent could be tested in further experiments. Nevertheless, the change of transfection reagent might not bring drastic increase in siRNA intake, as both RNAiMAX and Stemfect are lipid particles and rely on the same biological mechanism.

6.3 RNA interference failed to knock down *CLDN19* expression

In fluorescence control images it can be seen that the fluorophores accumulate to cells (Figure 10, 5.1). Z-stack images were not taken, but the hypothesis is that these molecules stick to cell membranes and do not enter the cells. The problem is that fluorescent labeling can change cell responses and surface properties of the particles.[76] Consequently, fluorescence labeled particles are not entering cells as efficiently as non-labeled particles. Therefore, it was thought that the WB experiment of the cells transfected with siRNA against CL19 should be done, even though the fluorophore tagged siRNA did not have good intake efficacy.

RNAi with each three repetitions was proven insufficient with WB. In one of the experiments the CL19 band was relatively smaller in CL19 knockdown sample compared to control sample (data not shown). This was stated as nonsignificant finding because the house-keeping control β-actin band was also smaller in RNAi treated sample. Therefore, the fainted signal of CL19 band was stated to result from the cytotoxic effects and not the decreasing of the expression of the protein. In other experiments, there were no decrease in CL19 protein levels between RNAi samples and control samples. In the relative signal intensity bars (Figure 10 E, 5.1) for CL19 bar for day 5 cell harvest is relatively higher than others, which indicates higher CL19 protein level in that sample. It is not a reliable finding, as it would require day 5 control sample to verify the result. In addition, the intention was to decrease the protein level, therefore this ostensible increase in protein level is not of interest in this study.

In RNAi experiment, the protein half-life is crucial. The effect of siRNA is changing due to cell divisions and mRNA stability. If CL19 is produced and broken down in a dynamic manner with a fast turnover rate, the effect of RNAi can end relatively quickly.[77] If the cells are not harvested in a suitable time point, the knock-down effect can be missed. Therefore, it is remarkably important to find an optimal time point for cell harvest after RNAi. Half-lives for claudin-2 (CL2) and claudin-4 are reported to be 12 and 4 hours, respectively.[78] Therefore, it could be estimated that the half-life of CL19 protein is approximately in the same scale. In a previous study, parallel transfections were used against CL19 at time points of d0 and d3 and cells were harvested five days post-transfection.[2] With this approach the knock down of gene expressions was successful. It could be stated that the harvesting time points in this study, d3 and d5, would have been successful, if the siRNA had passed the cell membrane. Therefore, RNAi failed probably because of the poor intake of the siRNA.

It could be considered, whether nuclear-targeted siRNA delivery for long-term gene silencing could be used to study CL19's role in ciliogenesis. This protocol uses nanocarriers that consist dense shells for siRNAs and peptides that target the carriers to be transported to nucleus. siRNA can bind to target gene's promoter and knock down gene expression inside the nucleus. The knock down induced by this protocol can last even for 30 days, as shown with RNAi against Thymidine Kinase 1.[79] As hESC-RPE cells are hard to transfect, this kind of long-term gene silencing could be a tempting approach to test. Transfection was proven efficient while transfecting the cells one day after plating. If this long-term silencing is performed with good translocation rate to the nucleus soon after plating, the CL19 could be silenced efficiently for longer time periods. This approach could be used to target exact time when the ciliogenesis initiates. Nevertheless, it must be considered, whether knocking down CL19 for such a long period affects RPE properties. As CL19 is the most abundant tight junction protein in human RPE[6,36], its silencing can lead to drastic effects for example in morphology and functionality. This could also affect ciliogenesis in a way that it cannot be studied by this manner.

It was stated that the RNAi failed to produce CL19 knockdown cells and the physical effects of CL19 knockdown on primary cilia was not studied. With the remaining time reserved for this project, it was decided to focus on studying the localization of CL19 in primary cilia.

6.4 EMT altered claudin-19 localization but had no effect on primary cilia lengths

Finding CL19 localization site in primary cilia was one of the main aims of this project. This was of interest because the localization sites of ciliary proteins could give insights on the

protein's role in primary cilia. For example, actin binging proteins have been suggested to have a mechanosensitive role in primary cilia and they could have functions in cilia membrane dynamics.[60] Both primary cilia dysfunctions and *CLDN19* mutations have been connected to developmental diseases.[7,36] The actual localization site of the protein could help to study also the possible disease mechanisms, by giving more information about the protein and its function. ExM was used in making super resolution images of primary cilia. It is a novel technique that allows nanoscale resolution imaging with conventional diffraction limited microscopes.[57] Learning to expand the sample before conventional confocal imaging is easier and faster than learning to use complex super resolution microscopes.

The studies of the CL19 localization were started with optimization of ExM protocol for hESC-RPE cells. The crucial steps in ExM to be optimized were fixation and IF staining. Usage of 4% PFA resulted with stiff fixation, and the epithelium got ruptured during the expansion steps. Therefore, 1% PFA was preferred in ExM. Expansion fades the fluorescence as the gel causes some quenching. Thus, it is preferred to use as high antibody concentrations as possible. In this study, the antibody concentrations were doubled compared to their regular concentrations in conventional IF staining. From our previous data, we have seen that when RPE cells are rather fusiform, primary cilia tend to be drastically long and CL19 is observed in them. In general, fusiform cells are similar to cells that are in EMT. For that reason, EMT was induced to direct the RPE cells towards fibroblast direction using TGF-β2 treatment, to study if EMT directs CL19 to localize in primary cilia.

TGF-β signaling pathway has an important role in inducing EMT during development and different morphogenetic events, among other important functions. Transcription factors TGF-β1, TGF-β2 and TGF-β3 bind to the same receptor and induce similar downstream effects that lead to EMT.[80] In literature, RPE cells were directed to EMT with varying TGF-β2 concentrations and treatment times[61-63]. Most common concentration was 10ng/ml and treatment times were 24 and 48 hours. Nevertheless, this concentration was used to hf-RPE and ARPE-19 but it was thought to be too gentle treatment for our robust hESC-RPE. Therefore, 10, 30 and 60ng/ml concentrations were tested with exposure times of 24 and 72 hours. The progression of the EMT state was planned to be evaluated during the TGF-β2 treatment based on changes in cell morphologies and TEER values. The EMT state is thought to decrease the TEER values as tight RPE is disturbed by emerging fibrotic cells. However, Regea08/023 cells were not visible in phase-contrast images and morphology evaluation of Regea08/017 EMT state was challenging, as it was impossible to say whether fusiform cells resulted from TGF-β2

treatment or poor differentiation to RPE cells. There was a small decrease in TEER values between TGF-β2 treated cells and non-treated control cells, and 10ng/ml concentration seemed to decrease the TEER values more than 30ng/ml concentration. Nevertheless, the changes in TEER values were not considered significant as the starting TEER values were low to begin with because of the fusiform cells among RPE cells. Therefore, the EMT state evaluation relied on IF staining. The most promising effect was seen with 30ng/ml concentration for 24 hours exposure. This EMT induction set-up would have been chosen for further CL19 localization studies with ExM, if the study was continued.

The IF staining indicates how RPE cells were directed to EMT state as a response to TGF-β2 treatment. Interestingly, CL19 localized to primary cilia after the treatment, which was in concordance with our observations that rather fusiform RPE cells possess CL19 immunopositive primary cilia. The hypothesis was that CL19 could have a role in controlling cilia length, because in our previous studies exceptionally long primary cilia have often been CL19 immunopositive. This was not detected in this study, as there were no significant differences in primary cilia lengths between treated and non-treated groups, even though the boxplots show that there are some longer primary cilia in the group with highest TGF-β2 concentration (Figure 21, 5.3). Nevertheless, only a small fraction of cilia in TGF-β2 treated groups were CL19 immunopositive. This brings bias to the statistical testing as the test is actually investigating whether TGF-β2 treated cells possess longer primary cilia than non-treated cells. Therefore, the effect of CL19 positivity in primary cilia length does not become evident in this testing. The differences in primary cilia lengths should be studied more carefully between CL19 immunopositive and CL19 immunonegative primary cilia to make conclusions about CL19's role in elongation of primary cilium. Furthermore, this issue could be studied further with more mature RPE cells. Our previous data has suggested that mature hESC-RPE cells possess relatively short primary cilia (unpublished data). If this EMT induction experiment was repeated with more mature cells, the variation in length would be reduced and the lengthening effect would become more evident.

In addition, MDCK cells have been proven to possess CL2 positive primary cilia. It was stated that CL2 is not necessary in ciliogenesis as these cells produce also cilia that are CL2 negative.[53] However, cells may possess primary cilia that look rather normal, but are dysfunctional because ciliary protein composition is not normal. This can lead to ciliopathies.[39] Previous data from our group indicates that CL19 is in primary cilia in certain stages of cell maturation process and is absent from primary cilia in mature RPE cells (unpublished data). The suggestion of normal

primary cilia without CL2 might be that CL2 had already been removed from primary cilia. In addition, ARPE-19 cell line does not express CL19 and still possess normally looking cilia.[72] It cannot be stated that the role of CL19 is not in maintaining primary cilium by indicating that primary cilia look rather normal without CL19. The functionality of primary cilia should be investigated in order to verify CL19's role in primary cilium maintenance. Furthermore, the next step of this study could be to investigate CL19's possible role in ciliogenesis. It would require the RNAi to be optimized in the time point of 24 hours, to block the primary cilia formation before ciliogenesis begins.

ExM was proven to be an efficient tool to study ciliary protein localization as the results of ARL13B localization was comparable with a previous study about ciliary proteins.[60] In addition, based on the ExM images, CL19 is present as beaded-necklace arrays. The resolution of ExM could be efficient enough to study the issue whether CL19 is produced by either two adjacent cells or a single cell. This kind of trans interactions for claudin dimers between two adjacent cells are shown for claudin-1, CL2 and claudin-3[32], but not for CL19. It would be interesting to compare CL19 staining with ZO-1 staining to get more information on their locations compared one another. Furthermore, the high resolution also brought insight into whether the primary cilium was on the apical membrane of the cell or inside the cell in the same level with the tight junctions (data not shown). This method could be used in assessing the state of primary cilia, as the growing cilia in RPE are synthetized by the intracellular pathway. Therefore, the primary cilia that were observed in the level of tight junctions, presumably were cilia that were under construction.

Furthermore, there has been two recent studies indicating that CL19 has a role as a signaling molecule and it regulates pathways that control barrier properties in RPE.[36,72] While considering CL19's signaling molecule function and primary cilium's role as a signaling hub, it could be possible that CL19 could localize into primary cilium while it is functioning in regulating signaling pathways. The role as a signaling molecule controlling barrier properties could explain why CL19 is localized in primary cilia only occasionally. We have found CL19 in primary cilia during cell maturation as barrier properties were evolving, and epithelium was forming its cell-cell junctions. This observation is further demonstrated in a study, that indicated that the regulatory role of CL19 occurs before tight junctions are fully matured.[36] This study indicated how EMT process affects ciliary localization. As cells were becoming more fusiform, CL19 was located in primary cilia and the cells lost some of their cell-cell interactions. This indicates that CL19 might possibly control also the degradation of epithelial barrier. In a

previous study, it is shown that loss of cell-cell contacts leads to EMT and onset of proliferation of RPE cells[81], which differs from to this study's finding. This difference could be explained by different cell types used, as in this study the cells were hESC-RPE cells, and the other study had primary porcine RPE cells. Our hESC-RPE are more similar to fetal RPE cells than adult RPE cells, which could explain the difference in the findings. Nevertheless, the role of CL19 in regulating not only tight junction formation but also degradation seems like a promising alternative hypothesis for the ciliary localization of CL19.

All in all, this study obtained protocols to study ciliary localization of CL19 and its protein levels in cells. Further studies about CL19's role in primary cilia is still required as this study failed to indicate whether CL19 knockdown cells produce abnormal primary cilia. This study provided evidence for our hypothesis that EMT could affect CL19 ciliary localization, which indicates that there could be a biological reason for CL19 transient primary cilia localization.

7 Conclusion

The purpose of this study was to set up protocols for studying CL19 and its role in hESC-RPE primary cilia maintenance. WB, EMT induction and expansion microscopy were optimized and proved to be reliable in studying this issue.

This study indicated that EMT is a process that induces CL19's primary cilia localization. Due to this data and the similarity between ciliopathies and CL19 associated diseases, it is evident that CL19 somehow alters primary cilia. Further studies are needed to estimate the role of CL19 in hESC-RPE primary cilia.

References

1. Strauss O. The retinal pigment epithelium in visual function. *Physiol Rev*. 2005;85(3):845-881.

2. Peng S, Rao VS, Adelman RA, Rizzolo LJ. Claudin-19 and the barrier properties of the human retinal pigment epithelium. *Invest Ophthalmol Visual Sci*. 2011;52(3):1392-1403.

3. May-Simera H, Nagel-Wolfrum K, Wolfrum U. Cilia - the sensory antennae in the eye. *Prog Retin Eye Res*. 2017;60:144-180.

4. Nishiyama K, Sakaguchi H, Hu JG, Bok D, Hollyfield JG. Claudin localization in cilia of the retinal pigment epithelium. *Anat Rec*. 2002;267(3):196-203.

5. Jin M, Wang D, Xu W, Wang H, Cao Y. Claudin-7b and claudin-h are required for controlling cilia morphogenesis in the zebrafish kidney. *Mech Dev*. 2020;161. doi: 10.1016/j.mod.2019.103595.

6. Konrad M, Schaller A, Seelow D, et al. Mutations in the tight-junction gene claudin 19 (CLDN19) are associated with renal magnesium wasting, renal failure, and severe ocular involvement. *The American Journal of Human Genetics*. 2006;79(5):949-957.

7. May-Simera HL, Wan Q, Jha BS, et al. Primary cilium-mediated retinal pigment epithelium maturation is disrupted in ciliopathy patient cells. *Cell Reports*. 2018;22(1):189-205.

8. Gerdes JM, Davis EE, Katsanis N. The vertebrate primary cilium in development, homeostasis, and disease. *Cell*. 2009;137(1):32-45.

9. Marshall WF, Ishikawa H. Ciliogenesis: Building the cell's antenna. *Nature Reviews Molecular Cell Biology*. 2011;12(4):222-234.

10. Szalai E, Nickerson JM, Grossniklaus HE. RPE histopathology and Morphometry. In: Klettner A, Dithmar S, eds. *Retinal pigment epithelium in health and disease.* Springer Nature Switzerland AG; 2020.

11. Sparrrow J,R., Hicks D, Hamel C,P. The retinal pigment epithelium in health and disease. *Curr Mol Med*. 2010;10(9):802-823. doi: 10.2174/156652410793937813.

12. Ablonczy Z, Dahrouj M, Tang PH, et al. Human retinal pigment epithelium cells as functional models for the RPE in vivo. *Invest Ophthalmol Vis Sci*. 2011;52(12):8614-8620. https://doi.org/10.1167/iovs.11-8021. Accessed 2/24/2020. doi: 10.1167/iovs.11-8021.

13. Maminishkis A, Chen S, Jalickee S, et al. Confluent monolayers of cultured human fetal retinal pigment epithelium exhibit morphology and physiology of native tissue. *Invest Ophthalmol Vis Sci*. 2006;47(8):3612. doi: 10.1167/iovs.05-1622.

14. Kaarniranta K, Salminen A, Kauppinen A. Retinal pigment epithelium in Age-related macular degeneration. In: Klettner A, Dithmar S, eds. *Retinal pigment epithelium in health and disease.* Springer Nature Switzerland AG; 2020.

15. Wang H, Cui X, Gu Q, et al. Retinol dehydrogenase 13 protects the mouse retina from acute light damage. *Mol Vis*. 2012;18(108-09):1021-1030.

16. Reichhart N, Strauss O. Ion channels of the retinal pigment epithelium. In: Klettner A, Dithmar S, eds. *Retinal pigment epithelium in health and disease.* Springer Nature Switzerland AG; 2020.

17. Detrick B, Hooks JJ. The RPE cell and the Immune system. In: Klettner A, Dithmar S, eds. *Retinal pigment epithelium in health and disease.* Springer Nature Switzerland AG; 2020.

18. Skottman H. RPE and Stem cell therapy. In: Klettner A, Dithmar S, eds. *Retinal pigment epithelium in health and disease.* Springer Nature Switzerland AG; 2020.

19. Da Cruz L, Chen FK, Ahmado A, Greenwood J, Coffey P. RPE transplantation and its role in retinal disease. *Prog Retin Eye Res*. 2007;26(6):598-635. doi: 10.1016/j.preteyeres.2007.07.001.

20. Zarbin M, Sugino I, Townes-Anderson E. Concise review: Update on retinal pigment epithelium transplantation for Age-Related macular degeneration. *STEM CELLS Translational Medicine*. 2019;8(5):466-477. doi: 10.1002/sctm.18-0282.

21. Yvon C, Ramsden CM, Lane A, et al. Using stem cells to model diseases of the outer retina. *Computational and Structural Biotechnology Journal*. 2015;13:382-389. doi: 10.1016/j.csbj.2015.05.001.

22. Forest DL, Johnson LV, Clegg DO. Cellular models and therapies for age-related macular degeneration. *Disease Models & Mechanisms*. 2015;8(5):421-427. doi: 10.1242/dmm.017236.

23. Achberger K, Haderspeck JC, Kleger A, Liebau S. Stem cell-based retina models. *Adv Drug Deliv Rev*. 2019;140:33-50. doi: 10.1016/j.addr.2018.05.005.

24. Takahashi K, Yamanaka S. Induction of pluripotent stem cells from mouse embryonic and adult fibroblast cultures by defined factors. *Cell*. 2006;126(4):663-676. doi: 10.1016/j.cell.2006.07.024.

25. Jin Z, Okamoto S, Mandai M, Takahashi M. Induced pluripotent stem cells for retinal degenerative diseases: A new perspective on the challenges. *J Genet*. 2009;88(4):417-424. doi: 10.1007/s12041-009-0063-5.

26. Moradi S, Mahdizadeh H, Tomo Šarić, et al. Research and therapy with induced pluripotent stem cells (iPSCs): Social, legal, and ethical considerations. *Stem Cell Research & Therapy*. 2019;10(1):1-13. doi: 10.1186/s13287-019-1455-y.

27. Sean MW, Hochedlinger K. Harnessing the potential of induced pluripotent stem cells for regenerative medicine. *Nat Cell Biol*. 2011;13(5):497. doi: 10.1038/ncb0511-497.

28. Findley MK, Koval M. Regulation and roles for claudin-family tight junction proteins. *IUBMB Life*. 2009;61(4):431-437. doi: 10.1002/iub.175.

29. Lal-Nag M, Morin PJ. The claudins. *Genome Biol*. 2009;10(8):235. doi: 10.1186/gb-2009-10-8-235.

30. Liu F, Koval M, Ranganathan S, et al. Systems proteomics view of the endogenous human claudin protein family. *Journal Of Proteome Research; J.Proteome Res.* 2016;15(2):339-359. doi: 10.1021/acs.jproteome.5b00769.

31. Angelow S, Ahlstrom R, Yu ASL. Biology of claudins. *American journal of physiology.Renal physiology*. 2008;295(4):F867. doi: 10.1152/ajprenal.90264.2008.

32. Van Itallie C,M., Anderson JM. Claudin interactions in and out of the tight junction. *Tissue Barriers*. 2013;1(3). doi: 10.4161/tisb.25247.

33. Tsukita S, Tanaka H, Tamura A. The claudins: From tight junctions to biological systems. *Trends Biochem Sci*. 2019;44(2):141-152. doi: 10.1016/j.tibs.2018.09.008.

34. Rizzolo LJ, Peng S, Luo Y, Xiao W. Integration of tight junctions and claudins with the barrier functions of the retinal pigment epithelium. *Prog Retin Eye Res*. 2011;30(5):296-323.

35. Günzel D, Yu A. Claudins and the modulation of tight junction permeability. *Physiol Rev*. 2013;93(2):525. doi: 10.1152/physrev.00019.2012.

36. Wang S, Xu T, Peng S, et al. Disease-associated mutations of claudin-19 disrupt retinal neurogenesis and visual function. *Communications biology*. 2019;2(1):113-13.

37. Angelow S, El-Husseini R, Kanzawa SA, Yu ASL. Renal localization and function of the tight junction protein, claudin-19. *American journal of physiology.Renal physiology*. 2007;293(1):F166. doi: 10.1152/ajprenal.00087.2007.

38. Rizzolo L. RPE polarity and Barrier function. In: Klettner A, Dithmar S, eds. *Retinal pigment epithelium in health and disease.* Springer Nature Switzerland AG; 2020.

39. Satir P, Christensen ST. Overview of structure and function of mammalian cilia. *Annu Rev Physiol*. 2007;69:377-400.

40. Kim S,Brian David. Assembling a primary cilium. *Curr Opin Cell Biol*. 2013;25(4):506-511.

41. Garcia-Gonzalo FR, Reiter JF. Scoring a backstage pass: Mechanisms of ciliogenesis and ciliary access. *J Cell Biol*. 2012;197(6):697.

42. May-Simera HL, Kelley MW. Cilia, wnt signaling, and the cytoskeleton. *Cilia*. 2012;1(1):7.

43. Kobayashi T, Dynlacht BD. Regulating the transition from centriole to basal body. *J Cell Biol*. 2011;193(3):435-444.

44. Larkins CE, Aviles GDG, East MP, Kahn RA, Caspary T. Arl13b regulates ciliogenesis and the dynamic localization of shh signaling proteins. *Mol Biol Cell*. 2011;22(23):4694. doi: 10.1091/mbc.E10-12-0994.

45. Molla-Herman A, Ghossoub R, Blisnick T, et al. The ciliary pocket: An endocytic membrane domain at the base of primary and motile cilia. *J Cell Sci*. 2010;123(10):1785-1795.

46. Nozawa YI, Lin C, Chuang P. Hedgehog signaling from the primary cilium to the nucleus: An emerging picture of ciliary localization, trafficking and transduction. *Curr Opin Genet Dev*. 2013;23(4):429.

47. Nozawa, Yoko Inès|Lin,Chuwen|Chuang, Pao-Tien. Hedgehog signaling from the primary cilium to the nucleus: An emerging picture of ciliary localization, trafficking and transduction. *Curr Opin Genet Dev*. 2013;23(4):429-437.

48. Li HX, Li JH, Feng LM. Hedgehog signaling pathway as a therapeutic target for ovarian cancer. *CANCER EPIDEMIOLOGY*. 2016;40:152-157.

49. Spasic M, Jacobs CR. Lengthening primary cilia enhances cellular mechanosensitivity. *European cells & materials*. 2017;33:158. doi: 10.22203/eCM.v033a12.

50. Hassounah NB, Bunch TA, McDermott KM. Molecular pathways: The role of primary cilia in cancer progression and therapeutics with a focus on hedgehog signaling. *Clinical Cancer Research*. 2012;18(9):2429-2435.

51. Mukhopadhyay S, Rohatgi R. G-protein-coupled receptors, hedgehog signaling and primary cilia. *Semin Cell Dev Biol*. 2014;33:63-72.

52. Li HX, Li JH, Feng LM. Hedgehog signaling pathway as a therapeutic target for ovarian cancer. *CANCER EPIDEMIOLOGY*. 2016;40:152-157.

53. Larre I, Castillo A, Flores-Maldonado C, et al. Ouabain modulates ciliogenesis in epithelial cells. *Proc Natl Acad Sci U S A*. 2011;108(51):20591-20596. doi: 10.1073/pnas.1102617108.

54. Hongisto H, Ilmarinen T, Vattulainen M, Mikhailova A, Skottman H. Xeno- and feeder-free differentiation of human pluripotent stem cells to two distinct ocular epithelial cell types using simple modifications of one method. *Stem Cell Research and Therapy*. 2017;8(1):291-15.

55. Skottman H. Derivation and characterization of three new human embryonic stem cell lines in finland. *In Vitro Cellular & Developmental Biology.Animal*. 2010;46(3/4):206-209.

56. Toops KA, Tan LX, Lakkaraju A. A detailed three-step protocol for live imaging of intracellular traffic in polarized primary porcine RPE monolayers. *Exp Eye Res*. 2014;124:74-85. doi: 10.1016/j.exer.2014.05.003.

57. Asano SM, Gao R, Wassie AT, Tillberg PW, Chen F, Boyden ES. Expansion microscopy: Protocols for imaging proteins and RNA in cells and tissues. *Current Protocols in Cell Biology*. 2018;80(1).

58. Schindelin J, Arganda-Carreras I, Frise E, et al. Fiji: An open-source platform for biological-image analysis. *Nature Methods*. 2012;9(7):676-682.

59. González-Mariscal L, Garay E, Quirós M. Identification of claudins by western blot and immunofluorescence in different cell lines and tissues. In: Turksen K, ed. *Claudins. methods in molecular biology (methods and protocols).* Humana Press, Totowa, NJ; 2011:213-231.

60. Kohli P, Höhne M, Jüngst C, et al. The ciliary membrane-associated proteome reveals actin-binding proteins as key components of cilia. *EMBO Rep*. 2017;18(9):1521-1535.

61. Wei Q, Liu Q, Ren C, et al. Effects of bradykinin on TGF-β1-induced epithelial-mesenchymal transition in ARPE-19 cells. *Molecular Medicine Reports*. 2018;17(4):5878-5886. doi: 10.3892/mmr.2018.8556.

62. Cl C, Yh C, Tai MC, Liang CM, Dw L, Jt C. Resveratrol inhibits transforming growth factor-β2-induced epithelial-to-mesenchymal transition in human retinal pigment epithelial cells by suppressing the smad pathway. *Drug Design, Development and Therapy*. 2017;11:163-173.

63. Yao H, Li H, Yang S, et al. Inhibitory effect of bone morphogenetic protein 4 in retinal pigment epithelial-mesenchymal transition. *Scientific Reports*. 2016;6(1). doi: 10.1038/srep32182.

64. Mclane MW, Hatzidimitriou G, Yuan J, Mccann U, Ricaurte G. Heating induces aggregation and decreases detection of serotonin transporter protein on western blots. *Synapse*. 2007;61(10):875-876. doi: 10.1002/syn.20438.

65. Sagné C, Isambert MF, Henry JP, Gasnier B. SDS-resistant aggregation of membrane proteins: Application to the purification of the vesicular monoamine transporter. *Biochem J*. 1996;316 (Pt 3):825.

66. Morita K, Furuse M, Fujimoto K, Tsukita S. Claudin multigene family encoding four-transmembrane domain protein components of tight junction strands. *Proc Natl Acad Sci U S A*. 1999;96(2):511-516. doi: 10.1073/pnas.96.2.511.

67. Krause G, Winkler L, Mueller SL, Haseloff RF, Piontek J, Blasig IE. Structure and function of claudins. *BBA - Biomembranes*. 2008;1778(3):631-645.

68. Bass JJ, Wilkinson DJ, Rankin D, et al. An overview of technical considerations for western blotting applications to physiological research. *Scand J Med Sci Sports*. 2017;27(1):4-25. doi: 10.1111/sms.12702.

69. Parker C, Warren M, Mocanu V. Mass spectrometry for proteomics. In: Alzate O, ed. *Neuroproteomics.* CRC Press; 2010.

70. Chang B, Liu G, Yang G, Mercado-Uribe I, Huang M, Liu J. REDD1 is required for RAS-mediated transformation of human ovarian epithelial cells. *Cell cycle (Georgetown, Tex.)*. 2009;8(5):780.

71. Irudayanathan FJ, Wang X, Wang N, Willsey SR, Seddon IA, Nangia S. Self-assembly simulations of classic claudins-insights into the pore structure, selectivity, and higher order complexes. *The journal of physical chemistry.B*. 2018;122(30):7463. doi: 10.1021/acs.jpcb.8b03842.

72. Peng S, Wang S, Singh D, et al. Claudin-3 and claudin-19 partially restore native phenotype to ARPE-19 cells via effects on tight junctions and gene expression. *Exp Eye Res*. 2016;151:179-189.

73. Bordeaux J, Welsh A, Agarwal S, et al. Antibody validation. *BioTechniques*. 2010;48(3):197-209. doi: 10.2144/000113382.

74. Weiping W, Brautigan David L. Phosphatase inhibitor 2 promotes acetylation of tubulin in the primary cilium of human retinal epithelial cells. *BMC Cell Biology*. 2008;9(1):62. doi: 10.1186/1471-2121-9-62.

75. Hansson ML, Albert S, Gonzalez Somermeyer L, et al. Efficient delivery and functional expression of transfected modified mRNA in human embryonic stem cell-derived retinal pigmented epithelial cells. *J Biol Chem*. 2015;290:5661-5672.

76. Suutari T, Silen T, SŞen Karaman D, et al. Real-time label-free monitoring of nanoparticle cell uptake. *Small*. 2016;12(45):6289-6300.

77. McEwan IJ. *The nuclear receptor superfamily : Methods and protocols.* ; 2009. 10.1007/978-1-60327-575-0.

78. Van Itallie C, Colegio O, Anderson J. The cytoplasmic tails of claudins can influence tight junction barrier properties through effects on protein stability. *J Membrane Biol*. 2004;199(1):29-38. doi: 10.1007/s00232-004-0673-z.

79. Li N, Yang H, Yu Z, et al. Nuclear-targeted siRNA delivery for long-term gene silencing. *Chemical Science; Chem.Sci.* 2017;8(4):2816-2822. doi: 10.1039/c6sc04293g.

80. Xu J, Lamouille S, Derynck R. TGF-β-induced epithelial to mesenchymal transition. *Cell Res*. 2009;19(2):156. doi: 10.1038/cr.2009.5.

81. Tamiya S, Liu L, Kaplan HJ. Epithelial-mesenchymal transition and proliferation of retinal pigment epithelial cells initiated upon loss of cell-cell contact. *Investigative Ophthalmology and Visual Science*. 2010;51(5):2755-2763.